Alma Mater Studiorum – Università di Bologna

Dipartimento di Fisica e Astronomia "Augusto Righi"

Laurea Magistrale in Fisica del Sistema Terra

Evolution of climate feedbacks on multi-centennial timescales

Presentata da:

Deborah Rotoli

Relatore:

Dott. Paolo Ruggieri

Correlatori:

Dott. Federico Fabiano

Dott. Christian Rodehacke

Anno Accademico 2023 - 2024

Appello I

Abstract

The thesis focuses on the topic of climate feedbacks and their dependence on the state of the system and on time. In this work, six 1000 years-long coupled climate simulations with different forcing are analyzed. The feedback parameter varies across the simulations and with time, and the aim of this work is to figure out which processes influence most this behavior. Using the radiative kernels method, the feedback parameter has been decomposed into individual contributions: Planck, water-vapor, lapse-rate, albedo and cloud. The forcing and time dependence of each individual feedback has been investigated to understand which one gives the largest contribution to the non-linearity.

Regarding the forcing/warming dependence, while cloud and lapse-rate feedbacks show unclear responses to increasing forcing, there is a noticeable increase in the water-vapor feedback and a decrease in both Planck and albedo feedbacks.

The change of the feedbacks along the simulations seems mostly influenced by the cloud feedback, that increases with time. We also report an increase in the lapse-rate feedback, while Planck and albedo feedbacks decrease with time.

The climate model used in this study does not include a proper treatment of ice sheet dynamics. Since Earth System feedbacks might impact the climate on these timescales, it is important to understand whether they influence the results obtained. In the final part of this work, performed during a period abroad, there is an initial attempt to address this issue by using the Parallel Ice Sheet Model to run a 1000-year-long simulation of the Greenland ice sheet.

Contents

Chapter 1

Introduction

The Earth's climate is governed by the energy budget at the top of the atmosphere (TOA). It is therefore relevant to study the main flows of energy into and out of the Earth system, and how these energy flows are modified in response to a radiative forcing. The Earth's energy budget depends on many factors like greenhouse gases concentrations, surface albedo and clouds.

Fig.1.1 shows which are the components to take into consideration: the incoming solar radiation and the outgoing radiation, composed by the reflected solar radiation and the outgoing thermal radiation. Earth's energy budget includes, in fact, the internal flows of energy within the climate system. The surface energy budget consists of the net solar and thermal radiation as well as the non-radiative components such as the sensible and latent heat fluxes.

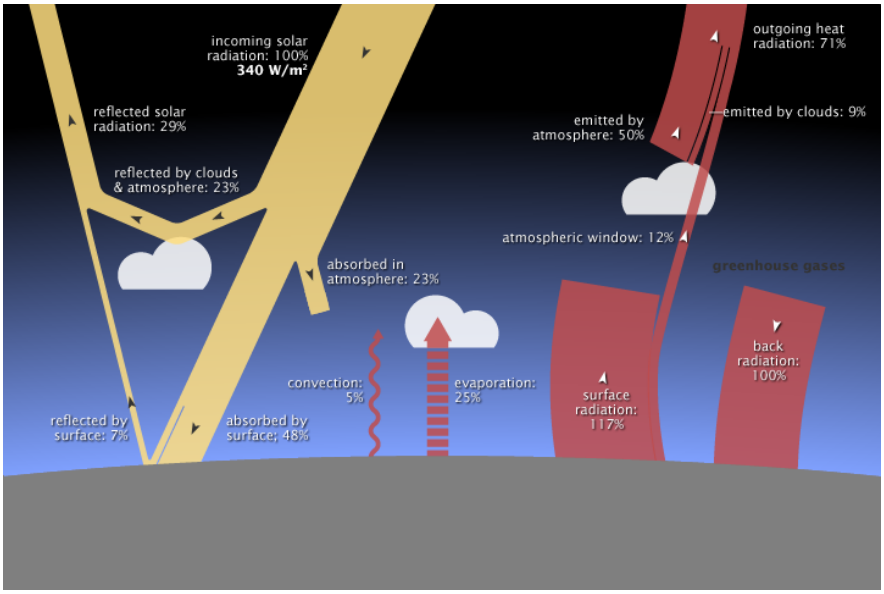

Figure 1.1: Earth energy Budget components

Climate sensitivity and feedbacks

The top-of-atmosphere (TOA) energy budget determines the net energy entering or leaving the climate system. When this budget changes due to human activities or, on paleoclimatic timescales, due to natural factors (known as 'radiative forcing'), the climate system responds by warming or cooling. The way the climate system reacts to a given forcing is influenced by various climate feedback mechanisms.

A typical approach to look at the response of the system to the radiative forcing is to consider the planetary energy balance at the TOA, represented as

$$R = F + \lambda \Delta T \tag{1.1}$$

where R is the net TOA radiative flux, F is the radiative forcing, λ is the radiative feedback parameter, and ΔT is the global mean surface air temperature anomaly. The sign convention is that R is positive downwards and λ is negative for a stable system.

Understanding the feedback mechanisms is crucial for predicting the trajectory of anthropogenic climate change and its potential impacts on the environment and society.

Feedbacks are due to the interactions between various components of the climate system that can either exacerbate climate change, leading to accelerated warming or cooling, or act as stabilizing factors that mitigate the effects of perturbations. These feedback loops can occur within the atmosphere, oceans, land surface, and cryosphere, influencing the overall climate response to external forcings (such as greenhouse gas emissions or changes in solar radiation).

As surface temperature changes in response to the TOA energy imbalance, many other climate variables also change, thus affecting the radiative flux at the TOA. The feedback parameter λ can then be decomposed into individual terms, such as Planck, water vapor, Albedo, lapse-rate and cloud.

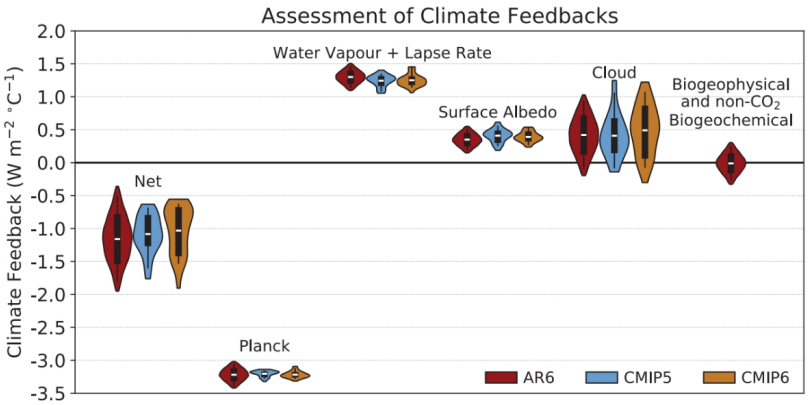

Figure 1.2: Global mean climate feedbacks assessed in the IPCC AR6 report and from abrupt4xCO2 simulations of the CMIP5 and CMIP6 multi-model ensembles. (IPCC 2021)

Fig.1.2 shows the individual feedbacks and the net feedback assessed in the IPCC AR6 report and from abrupt4xCO2 simulations of the Coupled Model Intercomparison Project - Phase 5 (CMIP5) and 6 (CMIP6) multi-model ensembles. As discussed above, some of these feedbacks are positive leading to an acceleration of the warming, and other negative:

- The most important negative feedback controlling the surface temperature of Earth is the Planck feedback. The Planck feedback is based on the Stefan–Boltzmann

law: it is the response of outgoing longwave radiation at TOA to a uniform perturbation in surface temperature and in the atmospheric temperature (applied to each vertical layer of the troposphere). The simple concept is that the warmer a body gets, the more energy it radiates.

- The water-vapor feedback quantifies the change in radiative flux at the TOA due to changes in atmospheric water vapor concentration associated with a change in global mean surface air temperature. It is necessary to look at it because with a warmer atmosphere more evaporation occurs from the ocean and from wet land surfaces. Thereby, on average, a warmer atmosphere will be a wetter one, this is also a consequence of the Clausius-Clapeyron relation, which states that the water vapor saturation pressure increases with increasing temperature. It means that the atmosphere will possess a higher water vapor content, since water vapor is the dominant greenhouse gas and the most important gaseous source of infrared opacity in the atmosphere, the result of rising temperatures will be a positive feedback. (Houghton 2015)

- The lapse-rate feedback quantifies the change in radiative flux at the TOA due to a nonuniform change in the vertical temperature profile. When the atmosphere warms more than the surface, the radiative energy flux to space increases relative to the radiation perturbation from a vertically uniform warming, yielding a negative feedback; alternatively, when the surface warms more than the atmosphere, the radiative energy flux to space decreases relative to the radiation perturbation from a vertically uniform warming, yielding a positive feedback (Boeke, Taylor, and Sejas 2021). The global lapse-rate feedback is small and negative in model simulations.

- The albedo is a measure of surface reflectivity. One of the primary physical

effects of the ice cover is the much higher albedo of ice and snow than all other surfaces (since they are powerful reflectors of solar radiation). The albedo of ocean surfaces at high latitudes is typically 10%, whereas a typical albedo for sea ice with a covering of snow at the same latitudes is 60%. The surface albedo contrast between coniferous forest and an ice sheet is equally great. As some ice melts, therefore, at the warmer surface, solar radiation which had previously been reflected back to space by the ice or snow is absorbed, leading to further increased warming. This is another positive feedback (Houghton 2015, Hartmann 1994).

- Clouds interact with the transfer of radiation in the atmosphere in two ways: firstly, they reflect a certain proportion of solar radiation back to space, so reducing the total energy available to the system; secondly, they act in a similar way to greenhouse gases by absorbing thermal radiation emitted by the Earth's surface below, and by emitting thermal radiation at a lower temperature. The effect that dominates for any particular cloud depends on the cloud temperature and on its detailed optical properties. The cloud feedback is very complicated as several processes are involved and represents the largest source of uncertainty in estimating the equilibrium climate sensitivity. Changes in cloud patterns due to warming will have different effects in various regions. Over subtropical oceans, the reduction of low clouds will lead to less reflection of solar energy, and the rise in the altitude of high clouds will trap more outgoing energy, both contributing to warming. In high latitudes, clouds will increasingly consist of water droplets instead of ice crystals, which will reflect more solar energy back into space, causing a cooling effect. Overall, improved understanding of cloud behavior indicates that future changes in clouds will likely result in additional warming, thus a positive net cloud feedback.

Identifying and quantifying these feedbacks is essential to improve the accuracy of climate models and refine projections of future climate scenarios.

Non-linearities in the climate response

Standard climate model simulations typically span only a few hundred years. However, feedback mechanisms operate on a wide range of timescales. These range from short-term responses to abrupt changes, such as shifts in cloud cover or ice-albedo feedbacks, to long-term processes like carbon cycle feedbacks. Modeling the long-term equilibration in response to radiative forcing perturbations is crucial for understanding numerous climate phenomena. This includes the evolution of ocean circulation, the dynamics of time- and temperature-dependent feedbacks, and the differentiation between forced signals and internal variability (M. Rugenstein et al. 2019).

One of the main research topics in climate change studies regards the projection of the future state of the climate under different scenarios of anthropogenic greenhouse gases (GHG) and aerosol emissions.

Shorter simulation's limitation is that they are transient simulations, in which the external forcing is continuously varying and the climate system is not able to catch up with the new forcing and remains far from the equilibrium. For this reason, exploring the final result of the anthropogenic perturbation to the climate system is fundamental to assess the likelihood of irreversible changes associated, for example, with ice sheets/glaciers melting.

The standard climate response model presented in Eq.1.1 relies on the assumption of a constant feedback parameter λ. However, Bloch-Johnson et al. (2021) showed that the feedback parameter is not a constant, but depends on the global warming level, on the warming pattern and on the external forcing imposed. Also, it is been proved that climate becomes more sensitive to greenhouse gas forcing as equilibrium is approached (Haugstad et al. 2017).

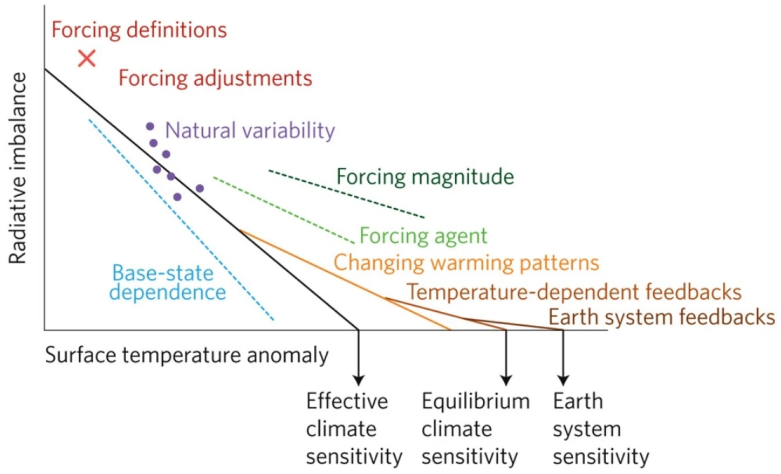

Figure 1.3: Conceptual illustration of the different processes, boundary conditions and forcings that can cause changes in the global feedback parameter (Knutti, M. A. A. Rugenstein, and Hegerl 2017).

The non-linearities in the climate response are summarised in Fig.1.3. It shows which are the major causes of change of the feedback parameter, indicated by the slope of the regressions. As we can see, the feedback parameter may depend on:

- the base-state of the climate;
- the forcing agent and magnitude;
- the timescale of equilibration, due to changes in warming patterns and temperature dependency of feedbacks.

This non-linear behavior has also been highlighted in Fabiano et al. (2023), they reported simulations spanning 1000 years, performed with EC-Earth3, which demonstrate changes in the climate feedback parameter throughout the simulations. Fig. 1.4 illustrates how this parameter varies from the first half to the second half of the simulation under different forcings.

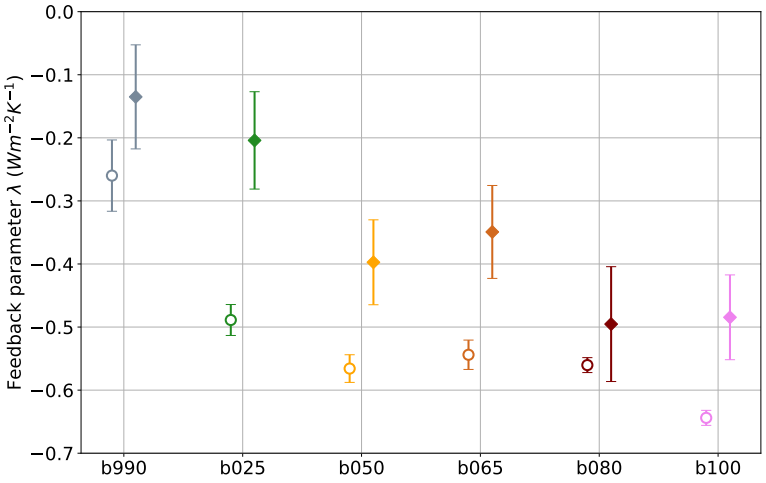

Figure 1.4: Climate feedback parameter estimated for the first (empty circle) and last (full) half of the simulations by Fabiano et al. (2023)

Starting from these same simulations, to better understand the behavior of the feedback parameter the purpose of this work is to split it into its components (Planck, Water-vapor, Lapse-rate, Albedo and Cloud feedbacks) using Kernels method (Soden et al. 2008), to look at their individuals behavior and figure out which one contributes most to the non-linearity. The analysis is presented in Section 3.2.

Earth system feedbacks

When long timescales are explored, slower components of the Earth system come into play. It takes, in fact, thousands of years to reach a new equilibrium and, by that time, long-term Earth system feedbacks, such as carbon cycle feedback, other biogeochemical feedbacks and ice sheets feedback will further affect climate. However, such feedbacks are not included in standard climate model simulations and poorly constrained (Knutti, M. A. A. Rugenstein, and Hegerl 2017).

As we can see in Fig.1.3 Earth system feedbacks may contribute to the change in the global feedback parameter. For this reason, transitioning from a climate model to an

Earth system model is ideal for a more comprehensive analysis of long-term feedback parameters, .

In this work, we will explore this topic by looking at the influence of ice sheets on the climate response.

Ice sheets affect Earth's radiative budget, hydrology, and atmospheric circulation due to their high albedo, low surface roughness, and elevation. They contribute freshwater to the oceans through calving and melting, influencing ocean circulation. Furthermore, changes in sea level caused by ice sheets alter land area and surface albedo.

On multi-centennial time scales the ice sheet feedback parameter is likely negative due to the impact on the ocean circulation, but on multi-millennial time scales the feedback parameter is very likely positive due to the land-ice albedo contribution (IPCC 2021).

In Section 4.1 we will explore the role of Earth-System feedbacks in the simulations presented in Fabiano et al. (2023) . The model used in that work does not include a proper treatment of Greenland and Antarctic ice sheets, and for this reason Fabiano et al. (2023) found complete melting of the ice in the region of Greenland for stronger forcing. In order to better understand the impact that this has on the climate response and on the feedback, we first tried to change the height of the water-equivalent amount of snow used in Greenland model, thus going from 10 to 1000 metres of snow on a fixed orography. However this approach cannot be considered a proper solution.

In the last section of this work a first attempt was made to have a more accurate description of the ice dynamics in the region of Greenland. The Parallel Ice Sheet Model (PISM) has been used to run a 1000 years long simulation of Greenland. The model, described in Section 4.1 does not take into account the two-way interactions between the ice sheet and the atmosphere, but allows a more realistic representation of the ice sheet response to the forcing applied.

Chapter 2

Methods and Data

In this section, we will delve into the methodologies employed in this study. We first focus on the decomposition of the feedback parameter into its individual components. Subsequently, attention will shift to the Greenland ice sheet model utilized for implementing ice dynamics.

2.1 Kernels method

As said above, we start from the planetary energy balance at the top of the atmosphere (TOA):

$$R = F + \lambda \Delta T$$

The aim of this work is to analyze the individual components (Planck, Water vapor, Cloud, Albedo and Lapse-rate) that make up the climate feedback parameter λ and quantify the contributors. To break down the feedback into individual components, we employ radiative kernels (Soden et al. 2008 Caldwell et al. 2016) that quantify the sensitivity of TOA radiation to small perturbations in surface and atmospheric temperature, water vapor, and surface albedo.

The method, used to calculate climate feedbacks, separates the feedback (for each

variable X) into two factors:

$$\lambda_X = \frac{\partial R}{\partial X}\frac{\partial X}{\partial T_s}. \tag{2.1}$$

The first term is the "radiative kernel" ($\frac{\partial R}{\partial X} = K$), where R is the net TOA radiation. It describes the change in TOA fluxes for a standard change in property X and depends only on the radiative algorithm and the base climate, such that the same kernel can be used for different climate experiments and models. The second term, the "climate response pattern" ($\frac{\partial X}{\partial T_s}$), is simply the change in the mean climatology of the feedback variable between two climate states. The product of these two quantities determines the climate feedback for that variable.

For each variable, anomalies are computed with respect to the mean climate of the preindustrial control simulation (piControl). For each month of the experiment, spatially-resolved kernels (computed by Soden et al. 2008 and Shell, Kiehl, and Shields 2008) are multiplied by the relevant climate field anomalies. Then, feedback processes with a vertical dimension, such as water vapor, lapse rate, clouds, and atmospheric Planck, are vertically integrated up to a time-varying tropopause, calculated as in Reichler, Dameris, and Sausen (2003). After that, a ten-year average was applied to eliminate the interannual variability patterns. The resulting fields, spatially averaged, are then regressed on global mean surface temperature (T_s) anomalies to yield the individual radiative feedback components λ_X.

Cloud feedback cannot be computed directly by multiplying the Soden et al. (2008) kernels with anomalies in the model-diagnosed vertical profile of cloud fraction because the radiative impact of clouds at a given level is strongly affected by vertical overlap with clouds at other levels. Cloud radiative effect (CRE) is defined as the difference between all-sky and clear-sky radiative fluxes at the TOA, so anomalies in CRE can be caused not only by cloud changes but also by changes in Planck, Water Vapor, Lapse-Rate, and Albedo, so these components have to be removed. The adjusted ΔCRE is

defined as:

$$\Delta R_{cld} = \Delta CRE - \sum_{i \neq cld} (\Delta R_i - \Delta R_i^0) \tag{2.2}$$

Where superscript 0 indicates calculations using clear-sky variables.

For some variables, time-average spatially resolved feedbacks have been computed dividing the corresponding ΔR_X (difference between the end and the beginning of the simulation) by the change in the global mean surface temperature.

Data

The feedback analysis was structured into distinct stages. Firstly, we initiated with the validation of the kernel method mentioned above. Subsequently, this method has been applied to scenarios involving longer time scales. For the phase of validation the procedure described above is applied to a fully coupled GCM (General Circulation Model) experiment data in which atmospheric CO2 concentrations are abruptly quadrupled from their preindustrial concentrations and held fixed (abrupt-4xCO2).

After validation, the same method is applied to long time-scale simulations, those used in this work were performed by Fabiano et al. (2023). These have been performed using the EC-Earth3 climate model (version 3.3.3), a state-of-the-art Earth-system model. EC-Earth3 includes robust and validated components for the atmosphere, the ocean, the sea ice and land processes. The simulations use the standard CMIP6 resolution, corresponding to a horizontal resolution of approximately 80 km and 100 km in the atmosphere.

Six simulations have been used for the second phase of this work, each one lasting 1000 years. Each simulation is branched at a specific year from the CMIP6 historical or the SSP5-8.5 simulation and the GHGs and aerosol concentrations are kept fixed thereafter at the branching-year level. The final states represent the world we would have in the far future if the atmospheric concentration of GHGs and aerosols were suddenly stabilized. They correspond to 1990 (historical), 2025, 2050, 2065, 2080 and 2100 (SSP5-8.5)

conditions. In the following part we refer to a specific simulation as "b####".

Fig.2.1 shows the GTAS (global mean surface air temperature) anomaly with respect to the pre-industrial climate for the six runs. The warming continues in all experiments well after the abrupt stabilization of the GHG concentrations.

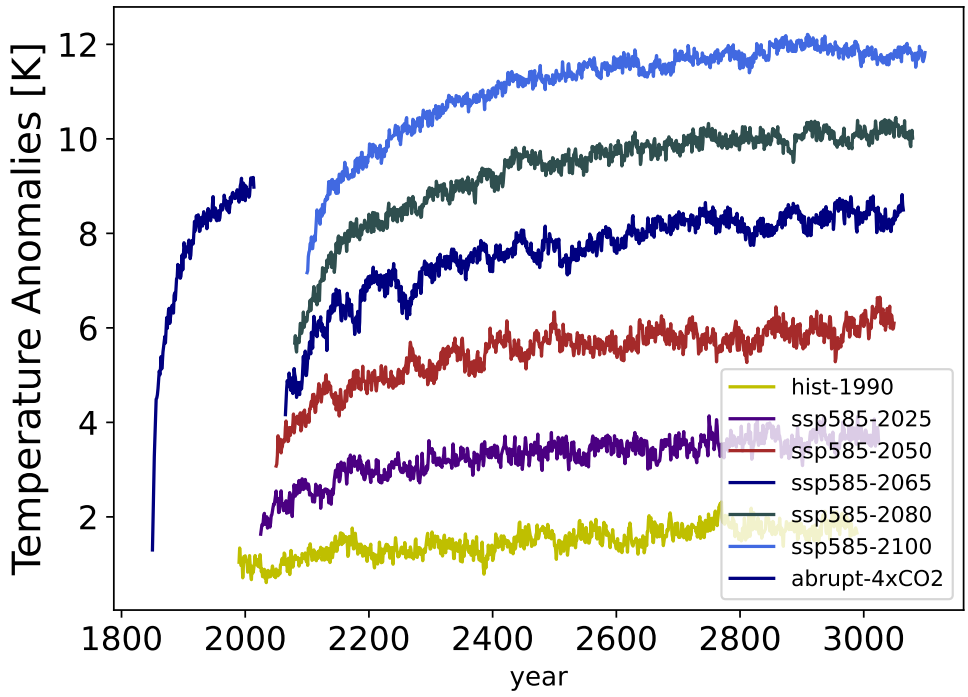

Figure 2.1: Global mean surface air temperature (GTAS) anomaly of all simulations($b1990$, $b2025$, $b2050$, $b2065$, $b2080$ and $b2100$) with respect to the pre-industrial mean climate

2.2 Ice-Sheets Models

As most current generation GCMs, this model version does not include a proper treatment of Greenland and Antarctic ice sheets. In fact, Greenland has been represented as mountains (with fixed orography) covered by a 10 meter water-equivalent amount of snow. For the simulations with stronger forcing ($b2080$, $b2100$) this leads to the

complete melting of Greenland and part of Antarctica.

To fix the problem, the first attempt was to increase Greenland snow cover from 10 to 1000 meters in $b2100$ simulation, using the same external forcing. The new simulation made with this modification is referred as $b00i$. These two simulations ($b2100$ and $b00i$) have been compared to assess whether the applied modification had an impact, particularly on the albedo feedback. Then, in the last section of this work we used a model that gives an accurate description of the dynamics of Greenland - the Parallel Ice Sheet Model (PISM) - to give an estimate of the land-ice albedo feedback. The objective was to initially assess the land-ice albedo feedback for b00i and subsequently compare it with the data acquired from PISM to see if the first results are realistic.

Parallel Ice Sheet Model (PISM)

PISM is a widely-used open-source software package used in climate science to simulate the past and future of glaciers and ice sheets, including the Earth's two large ice sheets in Greenland and Antarctica. It employs advanced numerical methods to simulate the ice behavior. PISM incorporates various physical processes such as ice flow, basal sliding, calving, and subglacial hydrology, enabling detailed and realistic modeling of ice sheet dynamics. With its parallel computing capabilities, PISM efficiently handles large-scale simulations, allowing us to investigate the complex interactions between ice sheets, climate, and the environment.

The evolution of ice sheets is mainly controlled by snow accumulation and ice loss through surface melting. Melt models generally fall into two categories: energy balance models, attempting to quantify melt as residual in the heat balance equation, and PDD (positive degree-day) models exploiting an empirical relationship between air temperatures and melt rates.

In this case, a PDD model has been used for the simulations. Although energy balance models more properly account for the processes determining melt, being more

physically based, they are often not practical due to large data requirements and uncertainties about spatial variability of some of these data. Hence, due to generally good performance, low data requirements and simplicity, temperature-index methods are most common (Hock 2003).

PDD

The degree-day model is a parameterization for the melt rate of snow and ice at the surface of an ice sheet or glacier. It is a simple, empirical relation which states that the melt rate is proportional to the surface-air temperature excess above $0°C$ (Calov and Greve 2005). The surface-melt rates is assumed proportional to the number of PDDs, which is given by an integral of surface-air temperature excess above $0°C$ in 1 year (Rogozhina and Rau 2014), so calculated:

$$PDD = \frac{1}{\sigma\sqrt{2\pi}} \int_0^A dt \int_0^\infty dTTexp\left(- \frac{(T - T_{acc}(t))^2}{2\sigma^2} \right) \tag{2.3}$$

Where t is the time, T the air temperature, T_{acc} is annual temperature cycle and σ is the temperature standard deviation.

Data

Using this method, a 1000 years long simulation has been run using $b00i$ values of surface temperature and precipitation as atmospheric forcing (it is important to keep in consideration that the $b00i$ simulation correspond to a shorter period 2100-2700). The standard deviation, while important due to its variation throughout the year, exhibits insignificant year-to-year changes. To streamline computational processes, the standard deviation from a single year is applied uniformly as a forcing for the entire duration of the simulation.

Chapter 3

Non-linearities in climate feedbacks

This Chapter presents the main results of this work regarding the warming/forcing and time dependence of individual climate feedbacks. It begins with the validation of the kernel method (Section 2.1) through comparison with reference data. Following its validation, the method is extended to analyze long-term data, with subsequent observation of the results. An in-depth analysis of individual feedback mechanisms follows thereafter.

3.1 Validation of kernels method

To validate the procedure illustrated in Section 2.1 it is been first applied on the fully coupled GCM (General Circulation Model) experiment data (abrupt-4xCO2). The feedbacks so calculated have been compared with those calculated (using the same approach) in Zelinka et al. (2020) as shown in Fig.3.1.
It should be specified that we used Soden et al. (2008) Kernels, while in Zelinka et al. (2020) they used Huang, Xia, and Tan (2017) kernels, because they yield the smallest residuals, but, as reported in Zelinka et al. (2020) all results are qualitatively unchanged between the two .

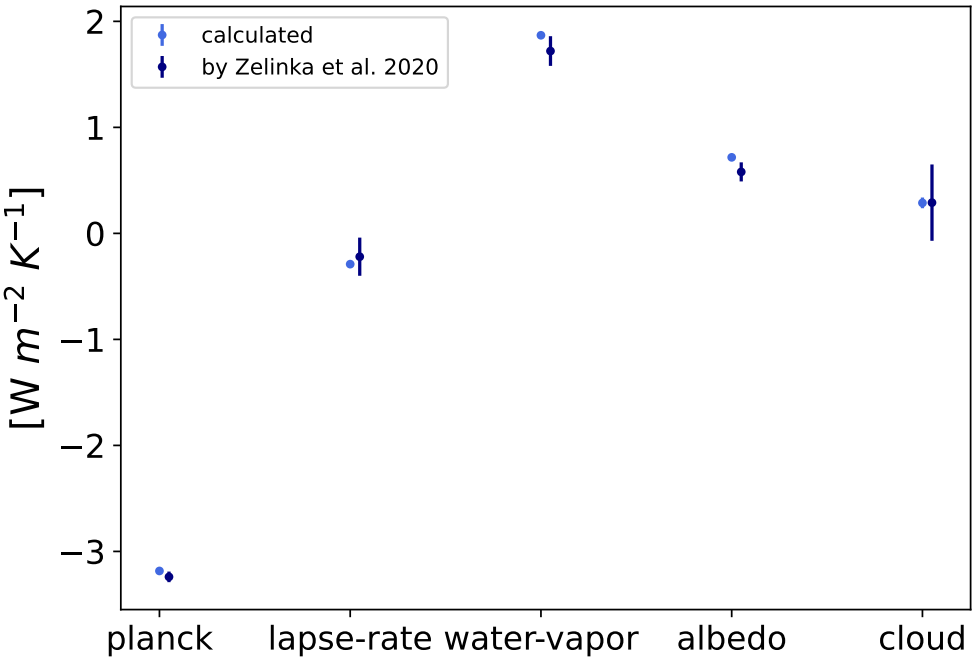

Figure 3.1: comparison between abrupt-4xCO2 calculated feedback and Zelinka et al. (2020) results

We can see that the computed values are in general agreement with the ones in Zelinka et al. (2020). However, some minor difference can be noticed. The feedbacks with the larger differences from the reference value, as can also be seen in 3.1, are cloud and albedo feedbacks.

There are some differences between the methodology used in this work and that used in Zelinka et al. (2020) that could explain these features. First of all, we used the whole 165-year long experiment, while Zelinka et al. (2020) only used the first 150-years. Another difference relates to the vertical integration, as in this work we integrated from a fixed surface pressure (1000 hPa) without readjusting for orography.

It is visible that the element with the biggest error is the cloud feedback, we can relate this feature to the method used to calculate it. As shown in Section 2.1 (Eq.2.1) it is calculated as a residual, the error propagation of all other feedbacks must therefore be

taken into account.

However, as we can see in Tab.3.1, the results obtained are in general agreement with the reference values, the procedure can therefore be considered valid.

	Calculated	Reference	Differences
Planck	-3.18 ± 0.02	-3.24 ±0.05	0.06 ±0.07
Lapse-rate	-0.29 ± 0.03	-0.2 ±0.1	-0.09 ±0.1
Water-vapor	1.86 ± 0.01	1.7 ±0.1	0.1 ±0.1
Albedo	0.71 ± 0.01	0.58 ±0.09	0.1 ±0.1
Cloud	0.28 ± 0.05	0.3 ±0.3	-0.002 ±0.3

Table 3.1: Individual feedback values and differences ($Wm^{-2}K-1$) with reference values (Zelinka et al. 2020)

3.2 Evolution of climate feedbacks in 1000 year-long climate simulations

In this section, we present the outcomes derived from applying the before mentioned procedure to the EC-Earth 1000-year long simulations. We particularly emphasize the examination of how individual feedbacks vary in response to different forcing factors and timescales. The procedure described in section 2.1, now validated, is applied to the 1000 years-long simulations above mentioned (b####).

Fig.3.2 shows individuals climate feedback of each simulation ($b1990$, $b2025$, $b2050$, $b2065$, $b2080$, $b2100$) and previously calculated abrubt-4xC02. The results of the long term simulations generally have values comparable with the abrupt-4xCO2 simulation. Anyway, some features can already be noticed.

The dispersion of values for each feedback, with some exhibiting more pronounced variations, is intricately linked to their sensitivity to both forcing and temperature differences.

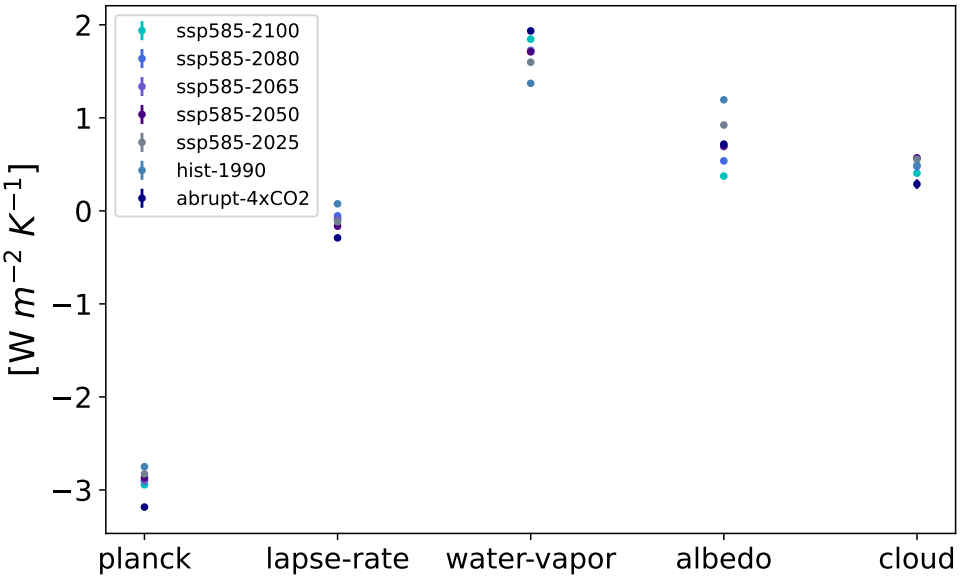

Figure 3.2: Comparison of individual feedbacks (abrupt-4xCO2 and 1000 years long simulations)

Indeed, Bloch-Johnson et al. (2021) has empirically demonstrated the presence of temperature and forcing dependencies within the feedback mechanisms. In our study, as outlined by Fabiano et al. (2023), the experimental configuration precludes the differentiation between forcing and temperature dependencies. However, it has been established that the temperature dependence of feedbacks holds paramount significance, thus forming the focal point of our analysis.

The feedbacks of utmost interest in Fig.3.2, namely albedo, lapse rate, and water vapor, exhibit the most significant spread, suggesting a potentially higher degree of dependency. Typically albedo feedback gives negative temperature dependence while water vapor feedback makes an increasing contribution with temperature. More details of the individual feedback will be discussed in the next section.

Before looking at the results, it is important to say that the first two simulations, $b1990$ and $b2025$, are the ones with the smallest imbalance, consequently they are also the most noisy.

3.2.1 Individual feedbacks analysis

In this section, the temperature and time dependence of each feedback is discussed. Temperature dependency is discerned through the observation of how the total feedback value varies across different simulations. Time dependency is assessed by calculating the feedback values separately for the first and second halves of the period, thereby observing variations over time.

Planck feedback

Fig.3.3 shows the value of Planck feedback for all simulations including abrupt-4xCO2 and the valued of first and second half of the period, in case of long-term simulations. The abrupt 4xCO2 simulation shows a more negative Planck feedback than all stabilization simulations. This variation could stem from two primary factors: firstly, differences in external forcing, as the *b*#### simulations includes additional greenhouse gases (GHGs) and aerosols; secondly, the abrupt-4xCO2 simulation captures responses at extremely short timescales, while all other simulations start from more equilibrated states.

Another important feature evident in the figure is that the value of the total planck feedback decreases (increases in magnitude) as the temperature of the simulation increase, suggesting a negative dependency of the feedback on temperature.

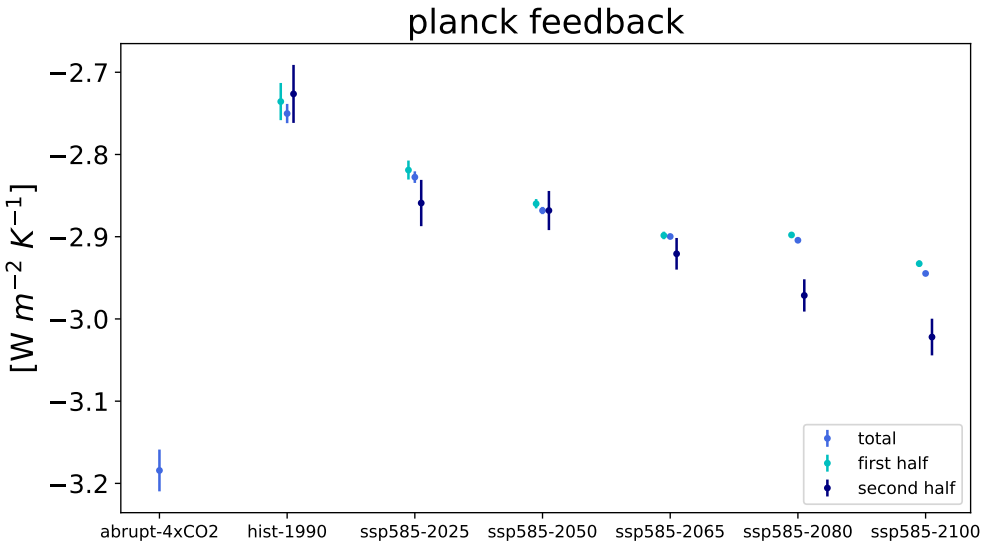

Figure 3.3: Planck feedback value of each simulation (including abrupt 4xCO2). For each simulation, the value of the whole period and the value for the first and second half of the simulation (500 year each) are shown.

The Planck feedback is considered as the sum of two factors: the surface Planck and the atmospheric Planck. The first refers to the variation of atmospheric temperature at each level (up to the tropopause), while the second to the variation of the surface temperature.

As shown in figures 3.4, 3.5, the surface Planck feedback does not change much, therefore it has less relevance in the total Planck feedback value change. It is clear that the atmospheric Planck decreases for increasing forcing and gives more contribution to the total value.

Fig.3.5 also shows that the difference between first and second half of the simulation increases with stronger forcing. Looking at Fig.2.1 we can see that those with the higher differences between first and second half are those whose surface temperature anomalies change the most throughout the simulation. Also, the warming pattern might play a role. The higher forcing simulations are warming more in the Southern ocean region, and this may increase the total Planck feedback (Bloch-Johnson et al. 2021).

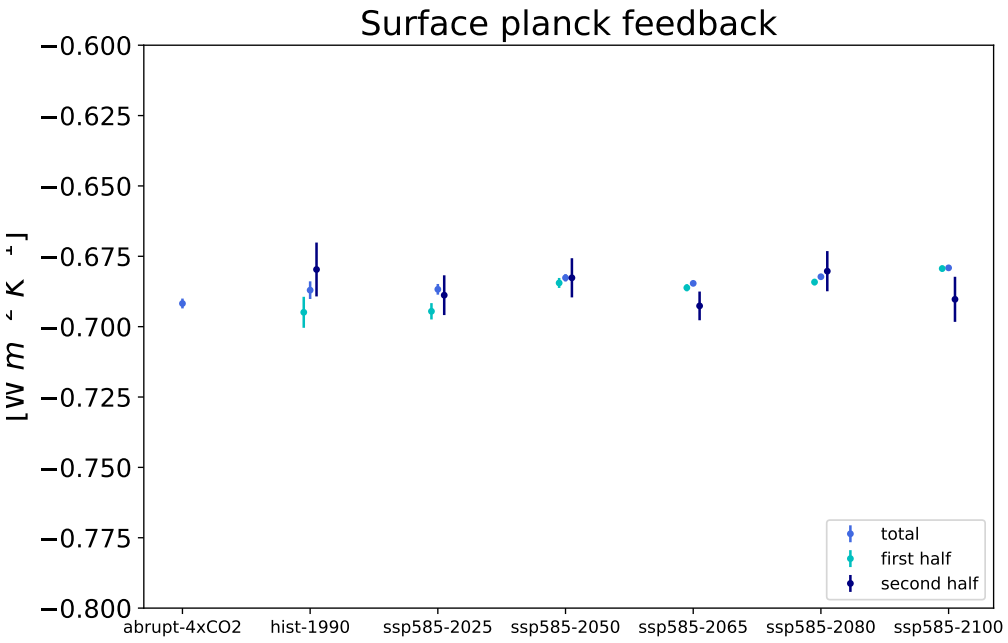

Figure 3.4: Surface Planck feedback value of each simulation (including abrupt 4xCO2). For each simulation, the value of the whole period and the value for the first and second half of the simulation (500 year each) are shown.

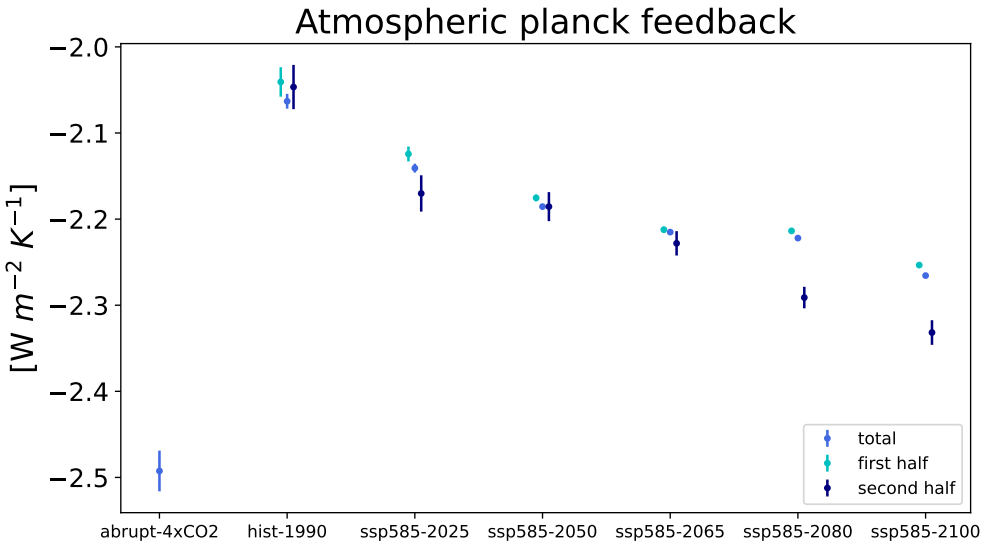

Figure 3.5: Atmospheric planck feedback value of each simulation (including abrupt 4xCO2). For each simulation, the value of the whole period and the value for the first and second half of the simulation (500 year each) are shown.

Water-vapor feedback

Fig.3.6 shows the value of the water vapor feedback for all simulations including abrupt-4xCO2 and the values of the first and second half of the period for the long-term simulations.

The Abrupt-4CO2 simulation exhibits higher water-vapor feedback value compared to other scenarios. The long-term simulation *b*2100 is the closest one, in fact it experiences temperature anomalies closer to Abrupt-4CO2, as shown in Fig. 2.1. Conversely, scenarios with lower temperature anomalies generally display lower water-vapor feedback values.

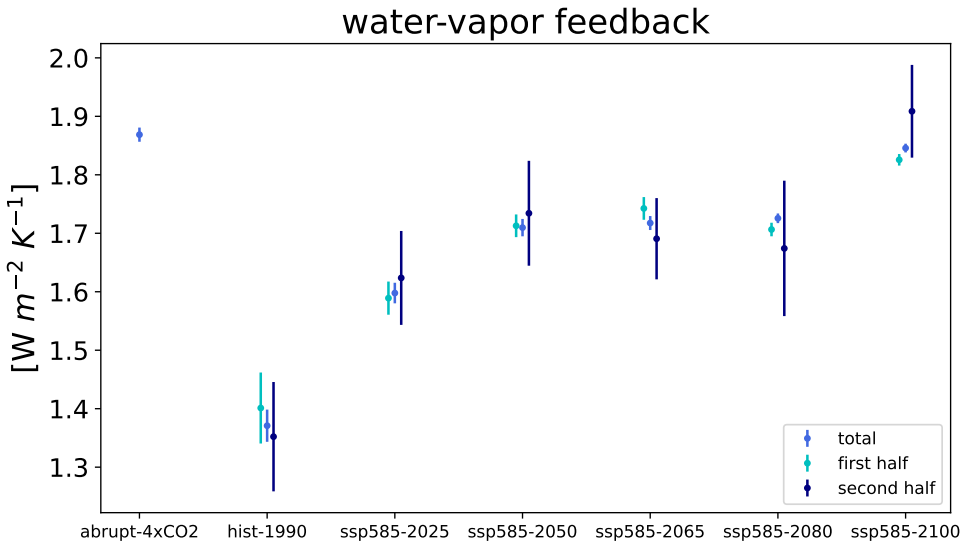

Figure 3.6: Water-vapor feedback value of each simulation (including abrupt 4xCO2). For each simulation, the value of the whole period and the value for the first and second half of the simulation (500 year each) are shown.

Fig. 3.6 illustrates an overall trend of increasing feedback total value with rising temperatures, except for the $b2065$ and $b2080$ simulations. However, this anomaly can likely be attributed to unaccounted factors such as other external forcing agents (other GHG and aerosols). The evolution of the water vapor feedback with time is unclear, with some simulations indicating a decrease while others show an increase in feedback values. Moreover, there is notable variability and uncertainty, particularly evident in the error margins during the second half of the simulations. Notably, the $b2100$ simulation stands out with a pronounced increase in feedback values during this period.

The overall increase of the feedback is also visible in the spatial patterns. Fig. 3.7 shows the time average water vapor feedback of $b2050$ and $b2100$ simulations. We can first notice a general increase in the feedback value from one simulation to the other. This is also shown in Fig.3.8, which represents the difference between the time-averaged water vapor feedback of $b2100$ and $b2050$. Increased feedback values are particularly

evident in the sub-tropical regions.

From the pattern we can notice some features. The tropical zone has very high feedback values, which then decrease going towards the poles. We see in the southern hemisphere areas with very small or negative water vapor feedback values, however, we can see that in the $b2100$ also in these areas the feedback becomes positive, consistent with more warming in the southern hemisphere in this scenario described in Fabiano et al. (2023).

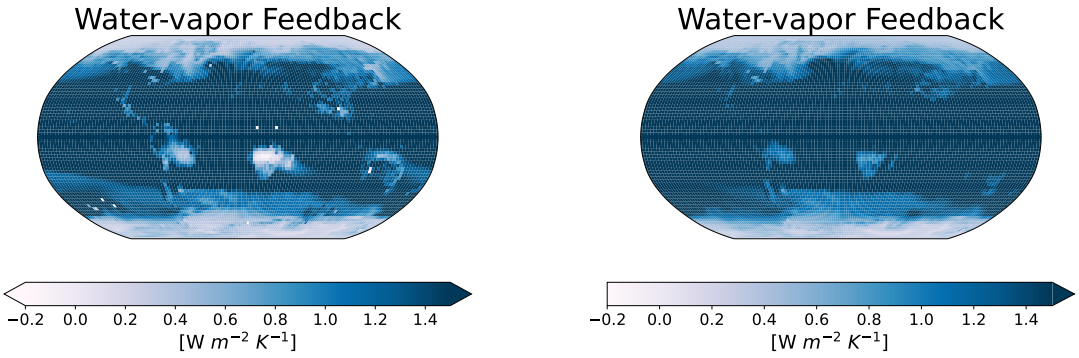

(a) *2050* **(b)** *2100*

Figure 3.7: Time averaged water vapor feedback pattern for $b2050$ and $b2100$.

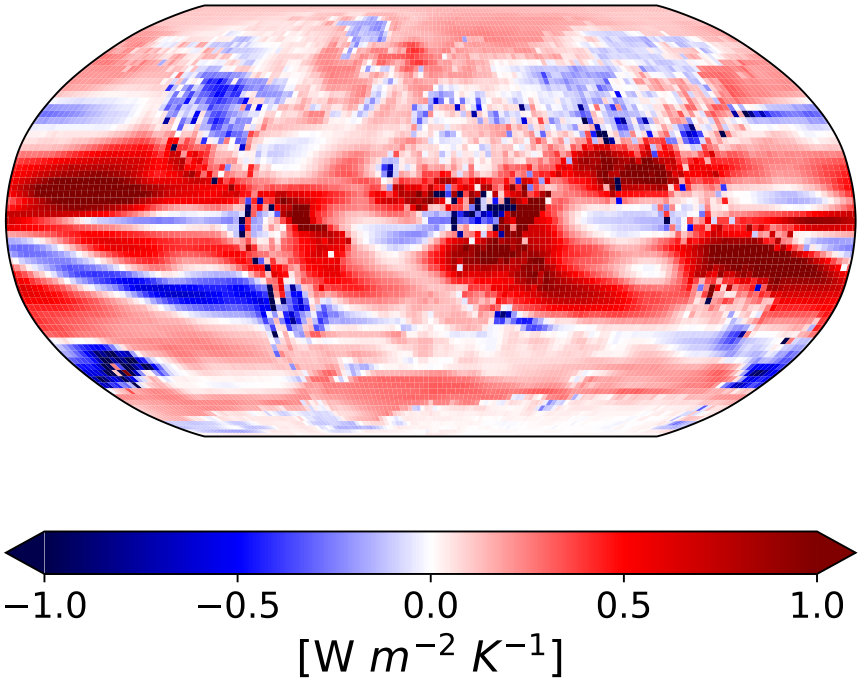

Figure 3.8: Pattern of the water vapor feedback difference between $b2100$ and $b2050$.

Cloud feedback

Fig. 3.9 shows the value of the cloud feedback for all simulations including abrupt-4xCO2 and the values of the first and second half of the period for the long-term simulations.

We can notice that abrupt-4xCO2 value is smaller than all other simulations, this might be due to the effect of aerosols or the different timescale.

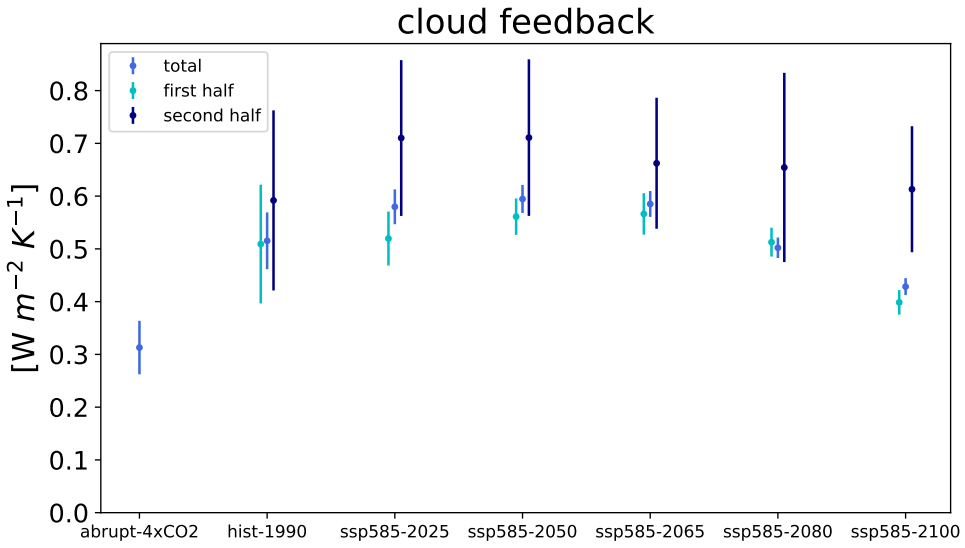

Figure 3.9: Cloud feedback value of each simulation (including abrupt 4xCO2). For each simulation, the value of the whole period and the value for the first and second half of the simulation (500 year each) are shown.

When examining the temperature dependence, a linear relationship cannot be identified. Notably, feedback values show an upward trend from $b1990$ to $b2050$, followed by a decline leading up to 2100.

Regarding the time-dependence of the cloud feedback, we notice that the value of the feedback in the first half of the period is smaller than the second half in all simulations, indicating that the cloud feedback becomes less stabilizing at long timescales. Also in this case, as for the Planck feedback, the difference is larger for the warmer simulations. As the climate warms, the progressive reduction of ice content in clouds relative to liquid leads to increased reflectivity and a negative feedback that restrains climate warming. A possible explanation for the observed behavior is that this feedback becomes smaller at long timescales, thus increasing the total net cloud feedback Bjordal et al. (2020).

Lapse-rate feedback

Fig. 3.10 shows the value of lapse-rate feedback for all simulations including abrupt-4xCO2 and the values of the first and second half of the period for the long-term simulations.

We can notice that Abrupt-4xCO2 values are lower (more negative) than long-term simulations. Also in this case, as for the cloud feedback, the behavior is non-linear. Notably, the b1990 feedback turns out to be slightly positive. Then, up to intermediate forcing (b2050), the feedback has a negative response to the increasing forcing and becomes negative. It then increases again for the simulations with stronger forcing, with values closer to zero.

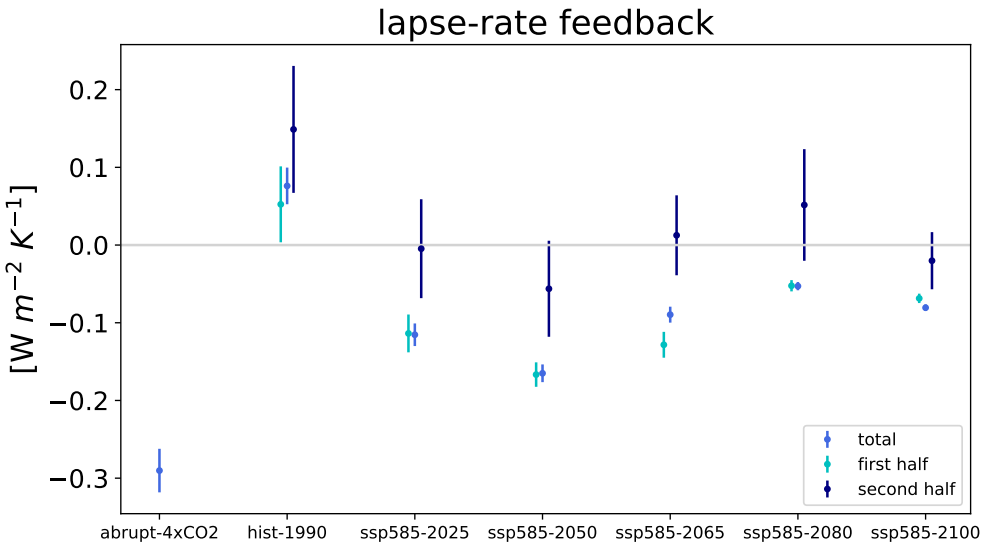

Figure 3.10: Lapse-rate feedback value of each simulation (including abrupt 4xCO2).For each simulation, the value of the whole period and the value for the first and second half of the simulation (500 year each) are shown.

The second half of the simulation has higher values for all the scenarios. This can be connected to the change in the warming pattern and to the delayed Southern Ocean response, which is visible in Fig.3.11, that shows the time-averaged feedback of the

$b2050$ and $b2100$ simulations.

In the Tropics the atmospheric temperature profile is constrained by approximate radiative-convection equilibrium. As the region gets warmer this lead to a negative lapse-rate feedback (Boeke, Taylor, and Sejas 2021).

In the Artic lapse-rate feedback is negative in summer and positive in fall/winter. As visible in the figure the average is positive.

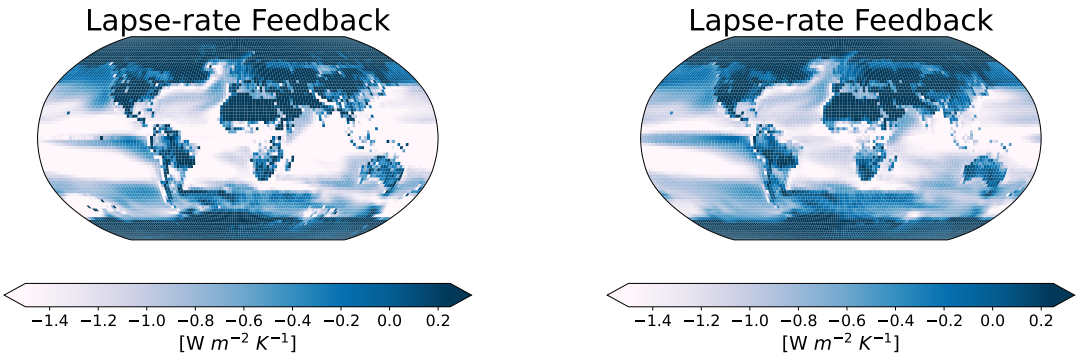

(a) *2050* **(b)** *2100*

Figure 3.11: Time averaged lapse-rate feedback pattern for $b2050$ and $b2100$

As can be seen in the maps (Fig.3.11), the lapse rate is influenced by the southern ocean warming, especially in the last scenarios. This feature is not recognizable in the abrupt simulation, Fig.3.12, given the short time span.

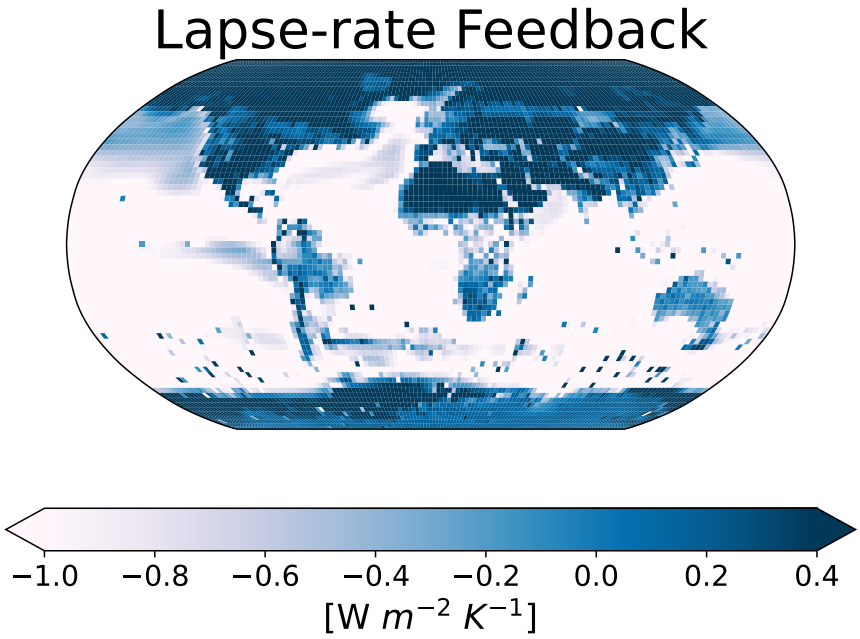

Figure 3.12: Time averaged lapse-rate feedback of abrupt-4xCO2 simulation

Albedo feedback

Figure shows the value of albedo feedback for all simulations including abrupt-4xCO2 and the values of the first and second half of the period, in case of long-term simulations.

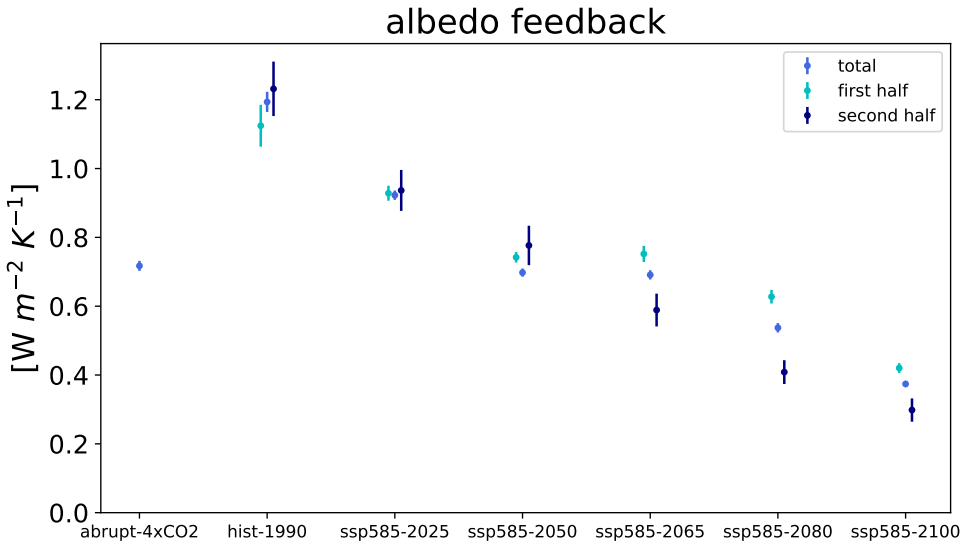

Figure 3.13: Albedo feedback value of each simulation (including abrupt 4xCO2). For each simulation, the value of the whole period and the value for the first and second half of the simulation (500 year each) are shown.

It is very clear that this feedback has a negative warming/forcing dependence, which we expect as higher temperatures decrease snow and sea-ice cover. There is no significant change at longer timescales in the albedo feedback for the $b1990$, $b2025$ and $b2050$ simulations. The difference between first and second half of the simulation increases with stronger forcing: for the $b2065$, $b2080$ and $b2100$ simulations the albedo feedback is reduced in the last 500 years.

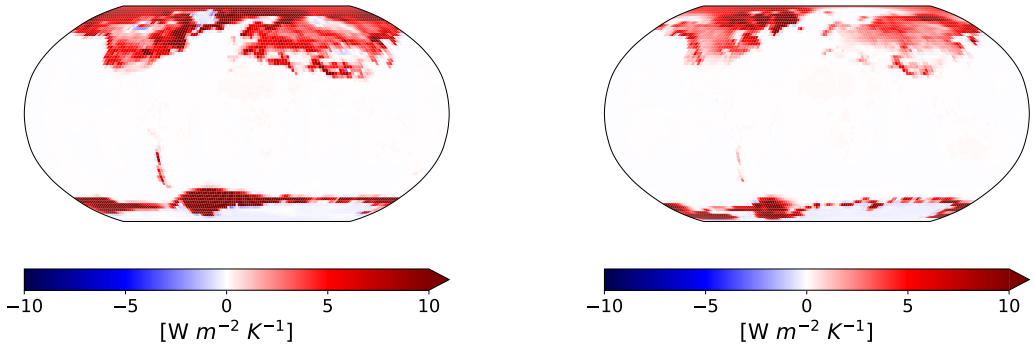

(a) $b2025$ **(b)** $b2100$

Figure 3.14: Time average albedo feedback pattern for $b2025$ and $b2100$

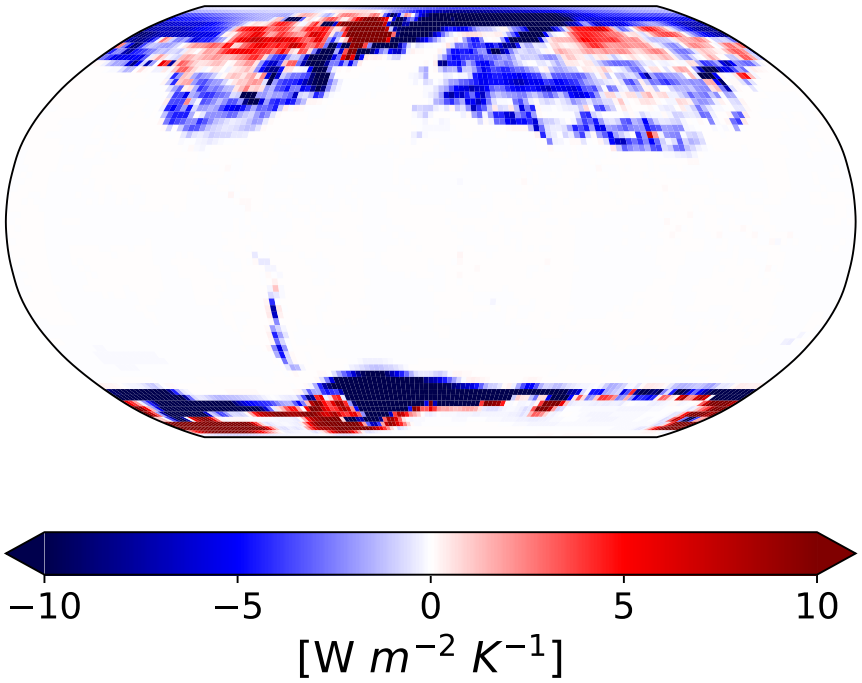

Figure 3.15: Time averaged difference between albedo feedback in $b2100$ and $b2025$

Looking at the temporal mean spatial patterns (Fig.3.14), we see that in the simulation with lower forcing ($b2025$) the feedback appears markedly amplified.

The most significant differences differences between the two simulations are observed in the polar regions and mostly due to the loss of sea-ice cover in $b2100$. This is visible in Fig.3.15, which represents the difference between the time-averaged albedo feedback of $b2100$ and $b2025$. Although there is a general decrease of the feedback, we can see an increase of the value in Greenland and Antarctica where the land ice melted.
As already mentioned, the difference of the albedo feedback between first and second half of the simulation increases with stronger forcing.
In the $b2100$ simulation, the albedo feedback value visibly decreases in the second half of the simulation, and this could be explained by the fact that, as also mentioned in Fabiano et al. (2023), in this simulation we observe the complete melting of all sea ice in the Northern Hemisphere and the majority of sea ice in the Southern Hemisphere. Additionally, the simulation depicts the total melting of Greenland's snow cover.

3.2.2 Time-dependence of climate feedbacks

Until now, emphasis was placed on how the various feedbacks varied according to forcing. Now, however, we want to observe the time-dependency, i.e. how the various feedbacks varied within the same simulation.
In the section above we discussed multiple times the increase of the difference between the first and second half of the simulations, often noticing that this difference increased with higher forcing.

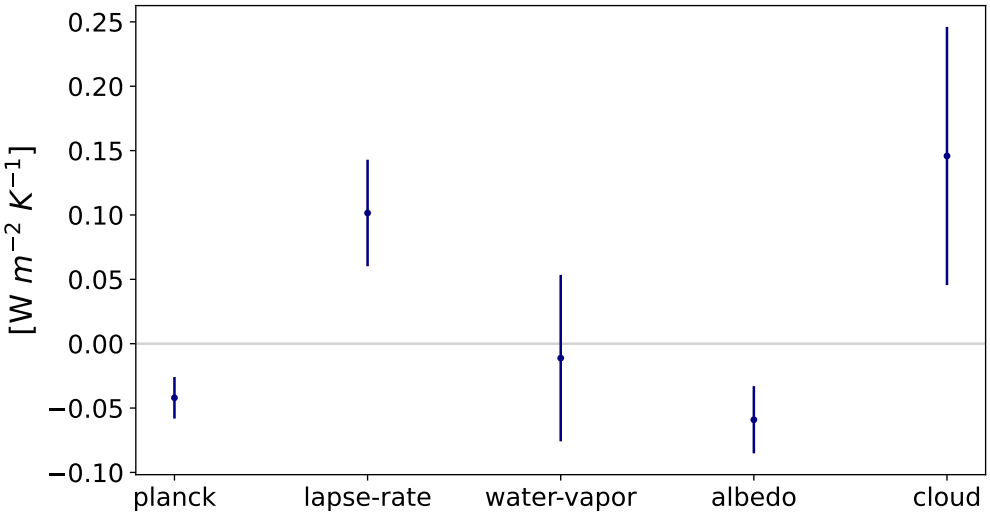

Figure 3.16: Averaged difference between first and second half of all simulations.

While in Fig.3.16 it's shown the averaged difference between first and second half of all simulations, we can see that some values are positive and others negative depending on whether the feedback decreases or increases along the simulation: if the feedback increases along the simulation then we will have a positive value, negative if it decreases. As per our interest, it's crucial to identify which of these differences is most pronounced, thus indicating the feedback that varies the most throughout the simulation. The cloud, lapse rate, and albedo feedbacks exhibit the highest variations. The cloud feedback also entails the largest uncertainty.

Regarding lapse rate, the substantial variation observed could be attributed to the "pattern effect". As highlighted by Bloch-Johnson et al. (2021) the non-linearity of the feedback may stem from the evolving warming patterns during the simulation. This evolution, primarily due to the delayed warming in regions of deep ocean heat uptake, contributes to the variability observed in lapse rate feedback. The change in the albedo feedback is likely due to a reduction in the snow, sea-ice and land-ice cover.

Chapter 4

Earth-System feedbacks: the role of the ice sheets

As explained in Section 2.2 , the standard EC-Earth3 model version does not include a proper treatment of Greenland and Antarctic ice sheets. These are represented as mountains (with fixed orography), which are covered by a 10 meter water-equivalent amount of snow. This, of course, represents a limitation in the model. The result is an overestimation of the albedo feedback over the ice sheets, since (as shown in Fabiano et al. (2023)) this simplistic representation results in a complete melting of the snow cover over Greenland and parts of Antarctica at high forcing (in particular in $b2100$) after a few centuries. Those regions are then left as mountains covered by bare soil, reducing the amount of reflected solar radiation.

To fix the problem, the first attempt was to increase Greenland snow cover from 10 to 1000 metres. The simulation made with this modification - using the same forcing as $b2100$ - is referred as $b00i$ and, for computational reasons, it does not extend for 1000 years but only up to 2700.

The most interesting feature is the change of the albedo feedback particularly noteworthy as Greenland and Antarctica retain their snow cover throughout the whole $b00i$ simulation.

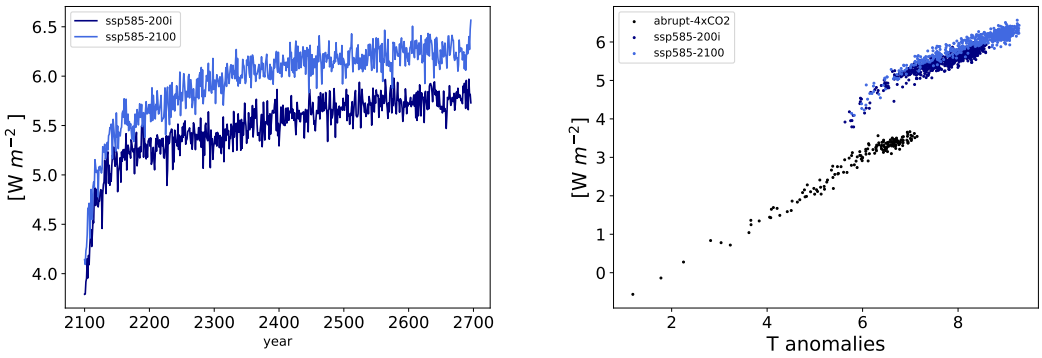

(a) *Albedo anomalies over time*

(b) *Albedo anomalies with respect to surface temperature anomalies*

Figure 4.1: Comparison between TOA radiative anomalies due to albedo differences in b2100 and b00i.

In Fig.4.3 we compare the net TOA anomaly due to the albedo change only, computed as the product of the response pattern and kernel before the regression with surface temperature anomalies. The modified model's simulation ($b00i$) has lower anomalies than $b2100$; anyway both $b2100$ and $b00i$ anomalies are higher than the ones from abrupt-4xCO2. It is also visible how the slope changes during the simulation, in contrast with abrupt-4xCO2 simulation which is quite linear. This reflects the evolution of the albedo feedback at longer timescales, with respect to abrupt-4xCO2, which is only 150 years long.

To give a closer look at this feature, Fig.4.2 shows the value of the albedo feedback for $b2100$ (full length, first and second half of the simulation) and for $b00i$ (rightmost point).

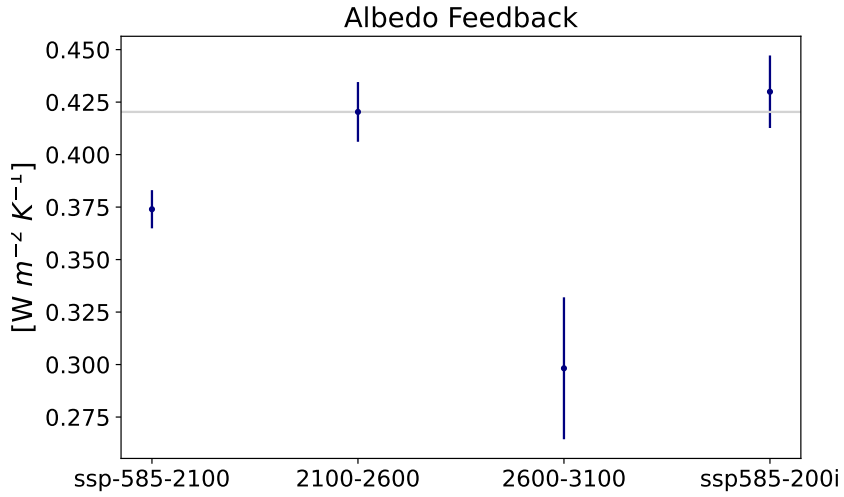

Figure 4.2: Albedo feedback values for different periods and time intervals.

Here it is visible that *b*00*i* has an higher albedo feedback with respect to *b*2100; however, since the *b*00*i* simulation is not 1000 years long but only 600, it is more convenient to look at the value of the feedback for the first half of the *b*2100 simulation. In this case, the two values are compatible inside the respective uncertainty.

To better understand the difference in slope between the two simulations shown in Fig.4.2 we look in more detail at the first 200 years of the simulation (2100-2300).

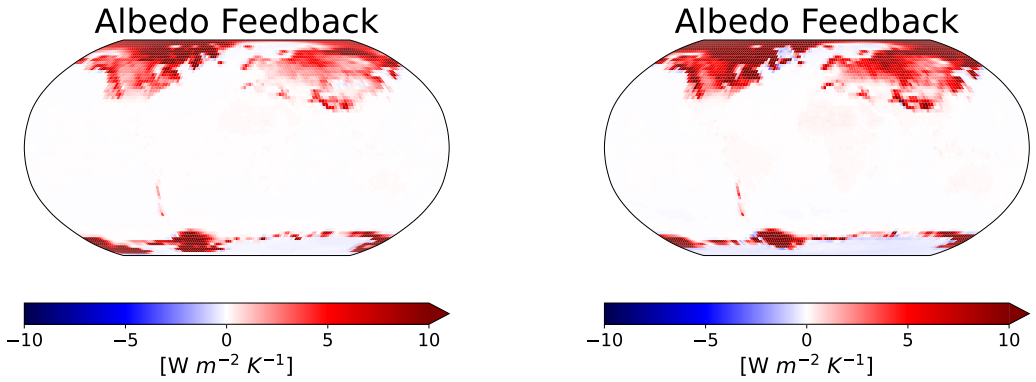

(a) *b2100 [2100-2300]* **(b)** *b00i [2100-2300]*

Figure 4.3: Time averaged albedo Feedback over the first 200 years of simulations (comparison between *b*2100 and *b*00*i*).

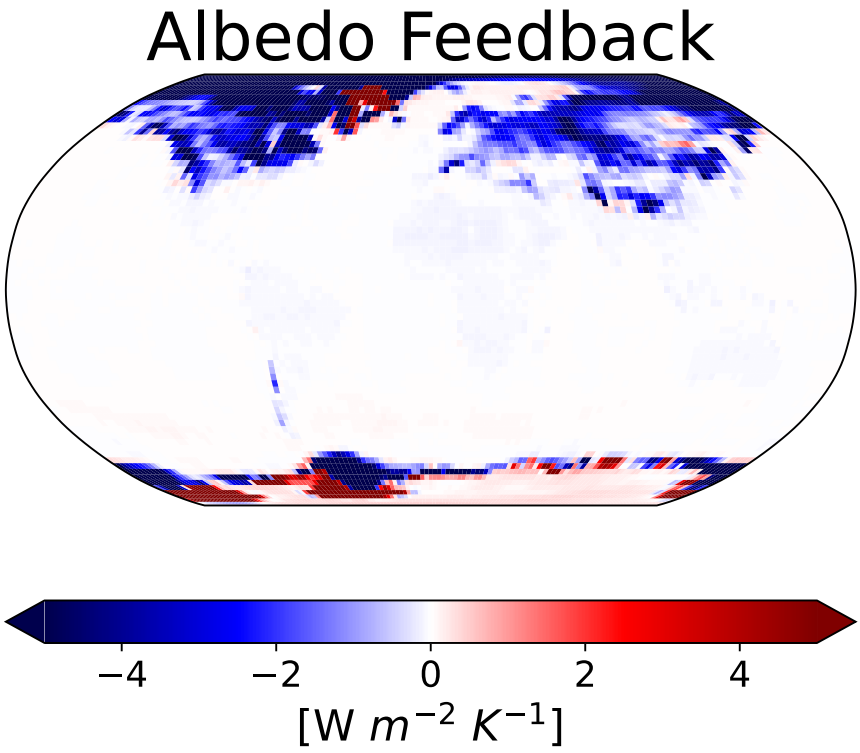

Figure 4.4: Difference between Time averaged albedo feedback over the first 200 years of simulation of $b2100$ and $b200i$.

In Fig.4.3 we see how the pattern are similar for the two simulations but large positive differences can be seen in the Greenland area and in the coast of Antarctica. This can also be observed in Fig.4.4, which shows the difference between time averaged albedo feedback over the first 200 years of simulation of $b2100$ and $b200i$. However, the positive difference is offset by a more negative response over land over much of the Northern hemisphere.

4.1 Numerical simulation of a dynamical ice sheet

In this section, we delve into a closer examination of Greenland to analyze the response of the ice sheet to the extreme $b200i$ external forcing using the dynamical ice sheet model PISM. The model effectively describes the ice dynamics and provides us with

data on the ice mass and glacierized area of the region we are focusing on.

The activities presented here have been undertaken during a period abroad at the Danish Meteorological Institute (DMI), which has a long experience in the study of the Greenland ice sheet. The aim of this activity is to compare the evolution of mass and ice-covered area with the results from the previously described EC-Earth simulations. We first describe the PISM simulation setup and then we will present the preliminary results.

Our objective here is to establish the simulation framework and provide an overview of its key aspects, as the comprehensive study of the model is still ongoing. The model presented here allows a better representation of the Greenland ice sheet dynamics, but still lacks a comprehensive account of all the interactions among different components of Earth system. To achieve a more precise representation, there is a need for a sophisticated Earth system model that integrates both ice dynamics and atmospheric such as coupled system for a former EC-Earth version 2 (Madsen et al. 2022).

The simulation

To describe the dynamics of the Greenland ice sheet, we ran simulations using PISM, based on a Positive Degree-Day (PDD) model as described in Section 2.2. These simulations use precipitation and temperature data from the $b00i$ simulation as forcing. Melting rates of snow and ice can be linearly related to the number of PDDs using degree-day factors for snow and ice, which are other major parameters controlling the output of PDD models.

PISM model also computes the solid (snow) precipitation rate using the air temperature threshold with a linear transition. All precipitation during periods with air temperatures above 2 °C is interpreted as rain; all precipitation during periods with air temperatures below 0 °C is interpreted as snow.

The PISM simulation has a resolution of 5 km resolution, which is higher than that of the EC-Earth model and output data. For this reason, the data used as forcing were first

regridded using bilinear interpolation, as will be discussed later in more detail.

For simplicity, the ice sheet simulations do not represent floating ice (e.g. ice shelves and ice tongues) and all ice is grounded, e.g. resides on land. Also, an ocean calving mask is set up, so that ice penetrating into the ocean is release as icebergs. Because of the change in the ice thickness, in PISM the elevation of the surface changes during the simulation, unlike the EC-Earth *b*00*i* simulation, which has a constant elevation. For this reason, the surface temperature must be corrected during the simulation: to do so, a fixed lapse-rate of 6 K/km is applied.

The output of the PISM simulation are yearly data of ice thickness, climatic mass balance, surface temperature, rate of change of the ice amount, ice mass and area. Upon regridding *b*00*i* data, some information is lost, particularly along the coastline, due to the resolution disparity between the two models used, as visible in Fig.4.5.

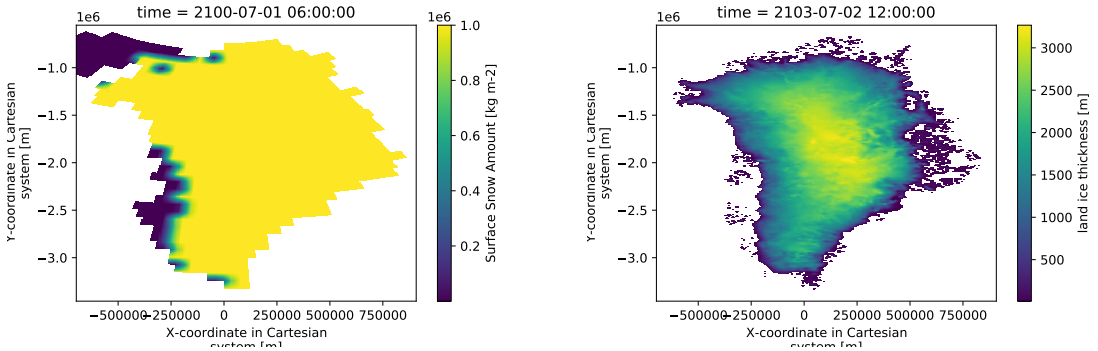

(a) *b00i* **(b)** *PISM*

Figure 4.5: Snow cover in the first timestep of the forcing (**a**) and ice cover at the beginning of the simulation (**b**).

Ice mass and extension

Below we present the first results obtained by running a simulation as described above. The results that we show here are preliminary and still under investigation, as we will comment later on.

Fig. 4.6 shows the evolution of ice mass during the simulation. It is visible that there is

an initial increase in ice mass and only after some centuries the mass decreases. This period of adjustment is visible in both glacierized area and mass change (Fig.4.6).

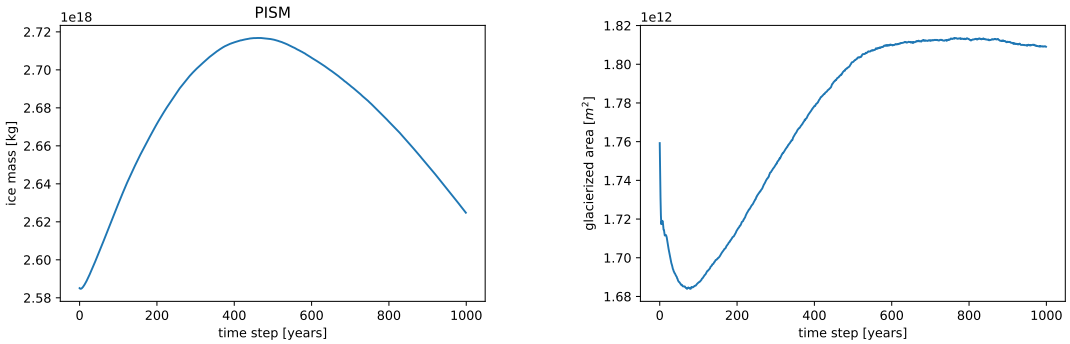

(a) *Ice mass* **(b)** *Glacierized area*

Figure 4.6: Variation of ice mass and glacierized area estimated with PISM simulation.

Something similar happens with the glacierized area. We can imagine that the initial decrease is due to the loss of information along the coasts and later, with melting in the central zone, a build-up occurs on the edges and the formation of thicker ice-sheets there, until a stabilisation is reached.

This is better shown in Fig.4.7, which shows the difference in thickness between last and first timestep of the simulation. It shows a loss of mass in the upper and central regions but an increment on the south and east coast.

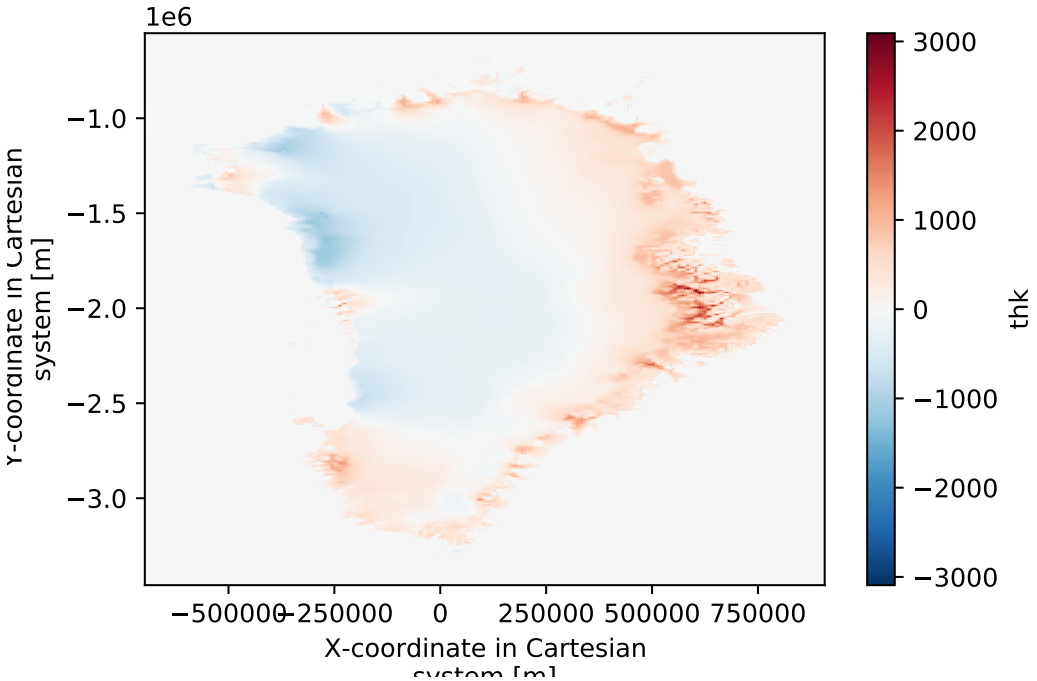

Figure 4.7: Difference in thickness (thk [m]) between last and first timestep of PISM simulation.

This behavior of the ice sheet was unexpected, since we are applying here a very strong external forcing ($b00i$). One hypothesis is that the difference between the climatology of the forcing $b00i$ and the initial condition used in the PISM setup gives rise to a period of adjustment, in which the ice sheet adapts to the new condition before it starts behaving as we expect it to. Another possibility is that the accumulation is caused by the precipitation, which is higher in this part of Greenland (Fig.4.8). In particular, the high snowfall rates in the south-eastern part is related to the Icelandic low pressure system and the general circulation triggering orographic precipitation (Schuenemann and Cassano 2009).

Also, when the accumulation occurs there is a change in elevation and this initiates a positive feedback loop: due to the lapse-rate adjustment of temperature, the temperature will decrease at the surface, leading to less melting for the reduced temperature so that the accumulation controls the surface mass balance.

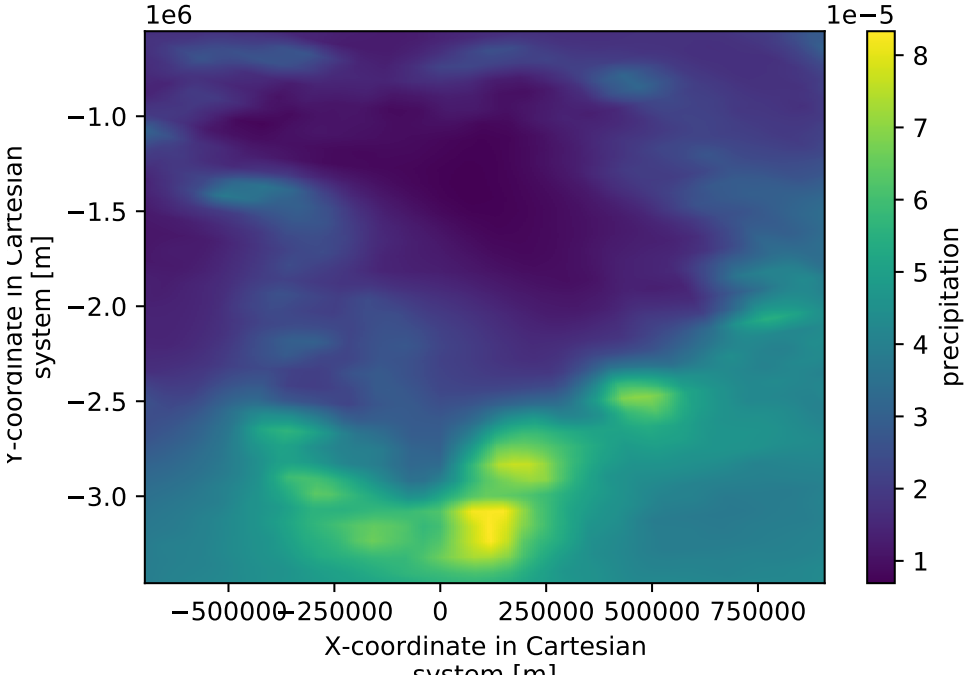

Figure 4.8: Time averaged precipitation $[kgm^{-2}s^{-1}]$ ($b00i$ Forcing)

4.2 Further work

To progress with this study, our aim is to conduct a comparative analysis of the results. To ascertain the reliability of the results derived from the $b00i$ simulation, it is imperative to compare the variations in ice mass and glacierized area (in the case of EC-Earth data, it will pertain to snow) with those calculated using PISM.

Here we perform a first comparison with the data obtained from the PISM simulation described above. Certain differences between the simulations must be taken into account: as far as $b00i$ is concerned, there is no data referring to ice but only to snow cover and surface snow amount; having used a PDD model, there is no radiative output from the simulations done with PISM.

We will then compare the ice cover and mass of the $b00i$, $b2100$ and PISM simulations. Looking at the mass in Fig.4.9, it can be seen that the $b2100$ has a different order of

magnitude from the other two, so although there are differences between PISM and *b*00*i*, surely this one is more reliable than the *b*2100.

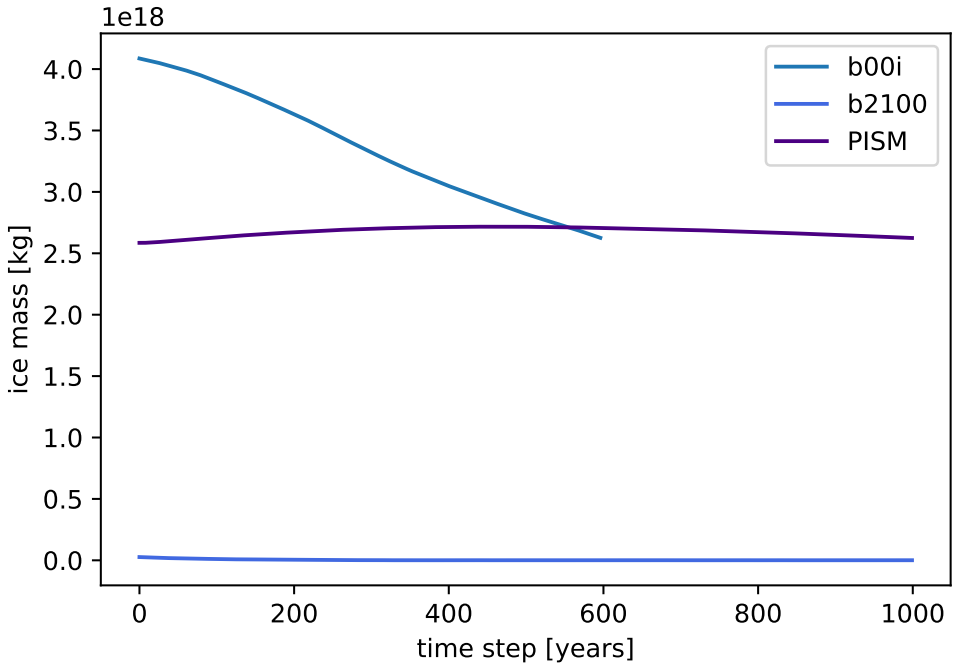

Figure 4.9: Comparison of Ice/snow mass variation between *b*00*i*, *b*2100 and PISM simulation.

As mentioned above in the case of the *b*2100 simulation there is an almost complete melting of Greenland as a result we see a much smaller covered area than in PISM. However, since the *b*00*i* simulation does not reach stability, it is not possible to make an accurate comparison between it and PISM.

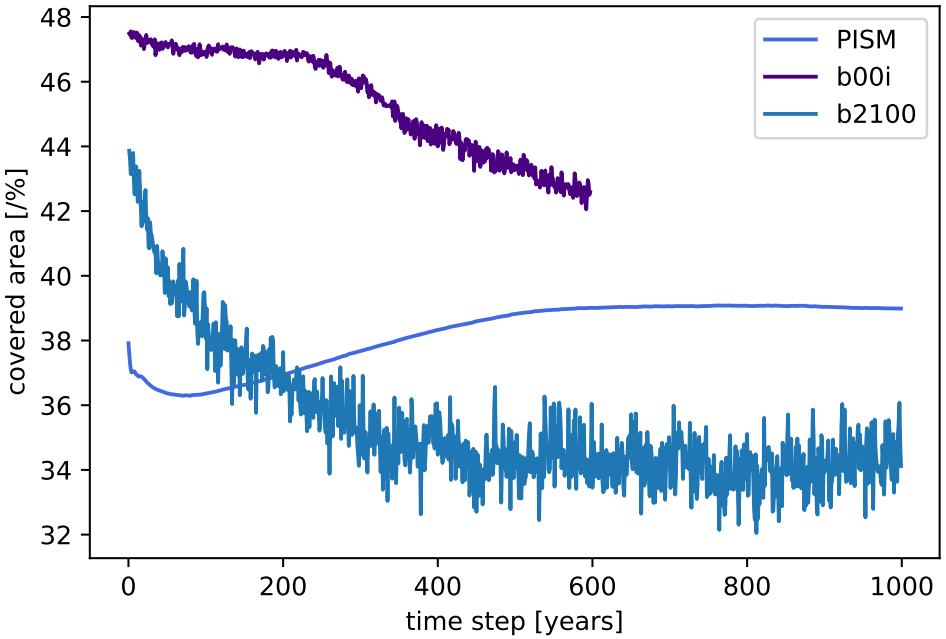

Figure 4.10: Comparison of glicierazied/snow covered area variation between $b00i$, $b2100$ and PISM simulation.

Given our specific focus on feedback values, particularly the albedo feedback, our primary interest lies in the variation of snow/ice cover. However, comparing the covered area among the three simulations proves challenging due to their notably distinct behaviors, as depicted in Fig.4.10.

To conduct a thorough analysis, it is necessary to comprehend the dynamics driving snow/ice accumulation in the eastern zone. Additionally, it may be necessary to refine certain features in the setup to enhance accuracy and ensure a more precise evaluation. Another alternative worth considering is to utilize an energy balance-based model instead of a PDD model. This approach would incorporate radiation data, enabling a direct comparison of the albedo feedback value. By implementing an energy balance model, we could more accurately assess the dynamics influencing snow/ice accumulation and gain insights into the intricacies of the albedo feedback mechanism.

Chapter 5

Discussion and Conclusions

In this work, we investigated the non-linearities in the climate response to external forcing, studying the evolution of individual feedbacks in a set of multi-centennial climate simulations. Six 1000 years-long coupled climate simulations with different forcing, presented in Fabiano et al. (2023), are analyzed. The feedback parameter varies across the simulations and with time, and we explored which processes influence most this behavior.

As a first step, we split the feedback parameter into its components - Planck, water-vapor, lapse-rate, albedo, and cloud - using the radiative kernels method. We then studied the contribution of each to the non-linearities in the response, with particular focus on identifying time and forcing/warming dependencies of these components.

To observe the warming/forcing dependence, for each feedback mechanisms we compare the values of the different simulations. To analyze the time dependence, we calculate the feedback separately for the first and second halves of the simulations, again considering all individual feedbacks.

As already reported in Bloch-Johnson et al. (2021) there is a feedback temperature dependence. In this work, looking at the individual contributions we noticed:

- the Planck feedback exhibit a negative dependence on forcing/warming. It becomes larger in magnitude (more negative) as the forcing increase, showing

values similar to those in the Abrupt-4xCO2 simulation for the scenarios with stronger forcing;

- the cloud feedback shows a non-linear behavior, first increasing and then decreasing with increasing forcing/warming and all simulations show a larger value than the abrupt-4xCO2 simulation;
- the lapse-rate feedback in all simulations has a smaller magnitude than in the abrupt-4xCO2, and also shows a non-linear behavior with respect to forcing/warming;
- the Albedo feedback exhibit a negative dependence on forcing/warming. It becomes smaller in magnitude (less positive) as the forcing increases, displaying lower values for the simulation with strong forcing compared to the Abrupt-4xCO2 simulation.
- Water-vapor feedback increases with stronger forcing, showing values similar to those in the Abrupt-4xCO2 simulation for the most intense forcing.

The temporal dependence is analyzed in Section 3.2.2, where we show how the individual feedbacks change during each simulation. Averaging the difference between first and second half of all simulations for each feedback (Fig.3.16) we were able to observe which influences most the temporal variation of the total feedback parameter. We found that:

- the cloud feedback increases during the simulations, it is also the one with the biggest difference. However, it's worth noting that it is also the one with higher error;
- the lapse-rate feedback is the second in terms of magnitude of the difference and it also increases during the simulations;
- the albedo feedback also shows big changes during the simulations, on average it tends to decrease along the simulations, more evident for larger forcing;

- the Planck feedback also shows on average a decrease for longer timescales, lower in magnitude with respect to the others;
- the water-vapor feedback has an average change close to zero.

Tab.5.1 summarizes the key results and general trends of the individual feedbacks discussed above.

	Sign (Abrubt-4xCO2)	**Forcing/warming dependence**	**Time dependence**
Planck	negative	decrease	decrease
Lapse-rate	negative	unclear	increase
Water-vapor	positive	increase	almost stable
Albedo	positive	decrease	decrease
Cloud	positive	non-linear	increase (high error)

Table 5.1: Main results regarding the non-linearities of individual climate feedbacks (trends refer to feedback parameters with the sign included).

In the last section of this work, we moved to analyze how Earth System feedbacks may influence the system response on these long timescales. First, the climate model limitations are discussed, regarding the unrealistic representation of ice sheets. Focusing on the land-ice albedo feedback, we examined how it changes when applying some modifications to the model in the Greenland area. However, an accurate description of this area, and glacierized areas in general, requires the use of an appropriate model. To address the inadequate treatment of glacierized areas and ice sheet dynamics, discussed above, we conducted a simulation using the Parallel Ice Sheet Model (PISM).
The simulation conducted with PISM, was used to compare the results obtained with the EC-Earth simulation with stronger forcing to validate their accuracy. In Section 4.1, it is discussed how PISM was used to generate a 1000-year-long simulation of this area. This represents a first step in moving from climate feedback to Earth system feedback. The simulation is not yet complete, and the work can still be improved. A good goal

would be to develop a model that accounts for the interactions between the various components of the system, thereby creating a comprehensive Earth system model.

Bibliography

[1] Jenny Bjordal et al. “Equilibrium climate sensitivity above 5°C plausible due to state-dependent cloud feedback”. In: *Nature Geoscience* 13 (2020), pp. 718–721. URL: https://api.semanticscholar.org/CorpusID:225072692.

[2] Jonah Bloch-Johnson et al. “Climate Sensitivity Increases Under Higher CO2 Levels Due to Feedback Temperature Dependence”. In: *Geophysical Research Letters* 48.4 (2021). e2020GL089074 2020GL089074, e2020GL089074. DOI: https://doi.org/10.1029/2020GL089074. eprint: https://agupubs.onlinelibrary.wiley.com/doi/pdf/10.1029/2020GL089074. URL: https://agupubs.onlinelibrary.wiley.com/doi/abs/10.1029/2020GL089074.

[3] Robyn C. Boeke, Patrick C. Taylor, and Sergio A. Sejas. “On the Nature of the Arctic’s Positive Lapse-Rate Feedback”. In: *Geophysical Research Letters* 48.1 (2021). e2020GL091109 2020GL091109, e2020GL091109. DOI: https://doi.org/10.1029/2020GL091109. eprint: https://agupubs.onlinelibrary.wiley.com/doi/pdf/10.1029/2020GL091109. URL: https://agupubs.onlinelibrary.wiley.com/doi/abs/10.1029/2020GL091109.

[4] Peter M. Caldwell et al. “Quantifying the Sources of Intermodel Spread in Equilibrium Climate Sensitivity”. In: *Journal of Climate* 29.2 (2016), pp. 513–524. DOI: 10.1175/JCLI-D-15-0352.1. URL: https://journals.ametsoc.org/view/journals/clim/29/2/jcli-d-15-0352.1.xml.

[5] Reinhard Calov and Ralf Greve. "A semi-analytical solution for the positive degree-day model with stochastic temperature variations". In: *Journal of Glaciology* 51.172 (2005), pp. 173–175. DOI: 10.3189/172756505781829601.

[6] F. Fabiano et al. "Multi-centennial evolution of the climate response and deep ocean heat uptake in a set of abrupt stabilization scenarios with EC-Earth3". In: *Earth System Dynamics Discussions* 2023 (2023), pp. 1–22. DOI: 10.5194/esd-2023-15. URL: https://esd.copernicus.org/preprints/esd-2023-15/.

[7] Dennis L. Hartmann. "Global Physical Climatology". In: 1994. URL: https://api.semanticscholar.org/CorpusID:128260404.

[8] A. D. Haugstad et al. "Relative roles of surface temperature and climate forcing patterns in the inconstancy of radiative feedbacks". In: *Geophysical Research Letters* 44.14 (2017), pp. 7455–7463. DOI: https://doi.org/10.1002/2017GL074372. eprint: https://agupubs.onlinelibrary.wiley.com/doi/pdf/10.1002/2017GL074372. URL: https://agupubs.onlinelibrary.wiley.com/doi/abs/10.1002/2017GL074372.

[9] Regine Hock. "Temperature index melt modelling in mountain areas". In: *Journal of Hydrology* 282.1 (2003). Mountain Hydrology and Water Resources, pp. 104–115. ISSN: 0022-1694. DOI: https://doi.org/10.1016/S0022-1694(03)00257-9. URL: https://www.sciencedirect.com/science/article/pii/S0022169403002579.

[10] John Houghton. *Global Warming: The Complete Briefing*. 5th ed. Cambridge University Press, 2015.

[11] Yi Huang, Yan Xia, and Xiaoxiao Tan. "On the pattern of CO2 radiative forcing and poleward energy transport". In: *Journal of Geophysical Research: Atmospheres* 122.20 (2017), pp. 10, 578–10, 593. DOI: https://doi.org/10.1002/2017JD027221. eprint: https://agupubs.onlinelibrary.

wiley.com/doi/pdf/10.1002/2017JD027221. URL: https://agupubs.onlinelibrary.wiley.com/doi/abs/10.1002/2017JD027221.

[12] IPCC. "The Physical Science Basis". In: *Climate Change 2021: The Physical Science Basis. Contribution of Working Group I to the Sixth Assessment Report of the Intergovernmental Panel on Climate Change*. Ed. by V. Masson-Delmotte et al. Cambridge, United Kingdom and New York, NY, USA: Cambridge University Press, 2021. Chap. 7, 7-1 to 7–78. DOI: 10.1017/9781009157896.009. URL: https://www.ipcc.ch/report/ar6/wg1/chapter/chapter-7/.

[13] Reto Knutti, Maria A. A. Rugenstein, and Gabriele C. Hegerl. "Beyond equilibrium climate sensitivity". In: *Nature Geoscience* 10.10 (2017), pp. 727–736. ISSN: 1752-0908. DOI: 10.1038/ngeo3017. URL: https://doi.org/10.1038/ngeo3017.

[14] M. S. Madsen et al. "The role of an interactive Greenland ice sheet in the coupled climate-ice sheet model EC-Earth-PISM". In: *Climate Dynamics* 59.3 (Aug. 2022), pp. 1189–1211. DOI: 10.1007/s00382-022-06184-6. URL: https://doi.org/10.1007/s00382-022-06184-6.

[15] Thomas Reichler, Martin Dameris, and Robert Sausen. "Determining the tropopause height from gridded data". In: *Geophysical Research Letters* 30.20 (2003). DOI: https://doi.org/10.1029/2003GL018240. eprint: https://agupubs.onlinelibrary.wiley.com/doi/pdf/10.1029/2003GL018240. URL: https://agupubs.onlinelibrary.wiley.com/doi/abs/10.1029/2003GL018240.

[16] I. Rogozhina and D. Rau. "Vital role of daily temperature variability in surface mass balance parameterizations of the Greenland Ice Sheet". In: *The Cryosphere* 8.2 (2014), pp. 575–585. DOI: 10.5194/tc-8-575-2014. URL: https://tc.copernicus.org/articles/8/575/2014/.

[17] Maria Rugenstein et al. “LongRunMIP: Motivation and Design for a Large Collection of Millennial-Length AOGCM Simulations”. In: *Bulletin of the American Meteorological Society* 100.12 (2019), pp. 2551–2570. DOI: 10.1175/BAMS-D-19-0068.1. URL: https://journals.ametsoc.org/view/journals/bams/100/12/bams-d-19-0068.1.xml.

[18] Keah C. Schuenemann and John J. Cassano. “Changes in synoptic weather patterns and Greenland precipitation in the 20th and 21st centuries: 1. Evaluation of late 20th century simulations from IPCC models”. In: *Journal of Geophysical Research: Atmospheres* 114.D20 (2009). DOI: https://doi.org/10.1029/2009JD011705. eprint: https://agupubs.onlinelibrary.wiley.com/doi/pdf/10.1029/2009JD011705. URL: https://agupubs.onlinelibrary.wiley.com/doi/abs/10.1029/2009JD011705.

[19] Karen M. Shell, Jeffrey T. Kiehl, and Christine A. Shields. “Using the Radiative Kernel Technique to Calculate Climate Feedbacks in NCAR’s Community Atmospheric Model”. In: *Journal of Climate* 21.10 (2008), pp. 2269–2282. DOI: https://doi.org/10.1175/2007JCLI2044.1. URL: https://journals.ametsoc.org/view/journals/clim/21/10/2007jcli2044.1.xml.

[20] Brian J. Soden et al. “Quantifying Climate Feedbacks Using Radiative Kernels”. In: *Journal of Climate* 21.14 (2008), pp. 3504–3520. DOI: https://doi.org/10.1175/2007JCLI2110.1. URL: https://journals.ametsoc.org/view/journals/clim/21/14/2007jcli2110.1.xml.

[21] Mark D. Zelinka et al. “Causes of Higher Climate Sensitivity in CMIP6 Models”. In: *Geophysical Research Letters* 47 (2020). URL: https://api.semanticscholar.org/CorpusID:213780557.